Super-regular breathers induced by the higher-order effects in coupled Hirota equations

Liuyi Pan,[1] Lei Wang,[1,*] and Lei Liu[2]

[1]*School of Mathematics and Physics, North China Electric Power University, Beijing 102206, People's Republic of China*

[2]*College of Mathematics and Statistics, Chongqing University, Chongqing 401331, People's Republic of China*

(Received 12 June 2024; accepted 8 August 2024; published 23 August 2024)

We study the intriguing dynamics of surper-regular breathers (SRBs) beyond the Manakov system. These SRB solutions are derived within the nondegenerate context. By employing the Darboux transformation, we obtain the exact expressions of the solutions for the vector SRBs in the coupled Hirota equations with the third dispersion, self-steepening, and inelastic Raman scattering terms. Based on such explicit formulas, we initially study the higher-order effects on their group velocities as well as the growth rate during the linear stage of modulation instability (MI). Additionally, we conduct an exploration of various mode excitations emerging during the nonlinear stage of MI. Our findings indicate that there exist significantly different wave modes from those in the Manakov system or the scalar nonlinear Schrödinger equation (NLSE). In particular, we refine existing formulas connecting the SRBs and MI in the nondegenerate regime, which eliminates the necessity to neglect higher-order terms from the Taylor expansion of α. Instead, we have used four different eigenvalues for a more comprehensive description. We also discuss the scalar SRB with two eigenvalues using wave component analysis. We finally excite, via numerical simulation initiated with localized periodic initial conditions, the vector SRBs and their transformed states. This study not only deepens our theoretical comprehension of SRB dynamics, but also illuminates potential avenues for future experimental investigations in this fascinating field.

DOI: 10.1103/PhysRevA.110.023523

I. INTRODUCTION

Breathers are known as the nonlinear coherent structures oscillating on the background plane waves, which describe the unique interactions and energy exchange with their backgrounds [1,2]. These waves have been observed in various experiments, including photonic crystal fibers [3], water wave tanks [4], nonlinear fiber optics [5], nearly conservative optical fibers [6], and so forth [2,7–13]. Generally speaking, there are two kind of breathers. One is the Akhmediev breather (AB), notable for its transverse breathing character while maintaining localization in other directions [14–16]. The other one is commonly recognized as the Kuznetsov-Ma soliton (KMS), distinguished by its periodicity in the propagation direction and transversal localization [15,17,18]. Both breathers can be converted into the Peregrine soliton in the limiting case of their periods being infinity [19,20]. The so-called Peregrine soliton is a special localized wave characterized by a rational form solution and can describe an isolated event such as rogue wave (RW), which "appears from nowhere and disappear without a trace" [21]. Additionally, more intricate breather structures can be produced by the nonlinear superpositions of the fundamental breathers in various significant physical phenomena such as breather wave molecules [6], chess-board-like interference patterns [13], vector breathers resonance [22,23], and even super-regular breathers (SRBs) [8,24,25]. The SRB describes a unique physical behavior where an initially small localized perturbation of the condensate gives rise to a pair of quasi-ABs propagating with different group velocities in the opposite directions [8]. All of these solutions are inherently related to the modulation instability (MI), which describes the instability of a constant background to long wavelength perturbations [16,26]. The exact correspondence between the fundamental localized waves and MI is elaborated in Refs. [27–29], with Ref. [27] extending this issue to the converted waves with higher-order effects. In addition, the concept of baseband MI has also been proposed, which reveals the link between MI and RWs. This also reveals that only this specific type of MI is capable of sustaining the formation of RWs [28–32].

In addition to the ABs and KMSs, the SRB holds significantly physical importance and can be viewed as the higher-order exact solutions of the scalar nonlinear Schrödinger equation (NLSE). The SRBs develop from the localized small perturbations at a certain moment of time [8,24] and then evolve into a pair of symmetric fundamental breathers propagating at a small angle to each other [8,24,25]. The explicit expression for this solution can mathematically be derived through the application of the dressing method in conjunction with the Jukowsky transform [8,24]. Further, the SRBs have been observed in two different branches of wave physics, namely, in optical and hydrodynamical experiments [25]. These results reported an interesting annihilation dynamics described by a pair of quasi-AB solutions. In fact, the AB solution describes a growth-return cycle evolved from a weak periodic perturbation during the nonlinear stage of elementary MI [3,14,16,25,26,33]. However, the higher-order MI formed by the nonlinear superposition of several elementary MI can exhibit more complex nonlinear dynamic behaviors in the

*Contact author: 50901924@ncepu.edu.cn

nonlinear stage, and the localized perturbation appears more universally in realistic physical contexts [33]. Such phenomena are usually described by the SRB solutions [8,24,25,34]. In fact, the initial stage of MI governed by the NLSE has been studied by linearizing the equation around constant backgrounds [14] while the characteristic of MI during the nonlinear stage is closely associated with two such kinds of breathers based on the analysis of discrete spectrum via inverse scattering transformation (IST) [35–38]. Other studies on the characteristics of nonlinear state of MI involve the continuous spectrum of IST. By studying the long-time asymptotics of the focusing NLSE on the infinite line with initial conditions tending to constant values at infinity [35–38], Biondini *et al.* shown that the x-t plane can be decomposed into left and right far-field regions during the nonlinear stage of MI, where the solution equals the condition at infinity to leading order up to a phase shift, and a central region in which the asymptotic behavior is described by slowly modulated periodic oscillations [38].

In addition to the above results, the conceptions of SRBs have been naturally extended to other physically important integrable systems [39]. For example, there are some novel characteristics during the nonlinear stage of MI as a result of higher-order effects, including the coexistence of a quasi-AB and a multipeak soliton, two multipeak solitons propagating in opposite directions, as well as a beating pattern followed by two multipeak solitons in the same direction [40]. Moreover, SRBs have also emerged within the framework of the complex modified Korteweg–De Vries (KdV) equation [34]. Unlike the conventional SRB composed of quasi-AB pairs in the NLSE [8,24,25], the SRBs within this equation can exhibit certain intriguing nonlinear structures, including the half-transition and full-suppression modes [34]. Recently, an exact link between the Zakharov-Gelash SRB and MI was established, revealing that the absolute difference in group velocities of the SRB aligns precisely with the linear MI growth rate [41]. This discovery marks a significant development in the SRB solutions, as it unveils, for the first time, the inherent relation between SRB and linear MI. Additionally, the SRBs, which are characterized by other nonlinear systems, including the self-induced transparency system [42], the derivative NLSE [43], the nonautonomous higher-order NLSE [44], and the Chen-Lee-Liu equation [43], can also exhibit some novel patterns, and the exact links between MI and the SRBs within these respective systems have been individually determined [43–45]. In very recent years, this understanding has broadened to include the vector fields consisting of two coupled wave components such as the coupled Maxwell-Bloch equations [42] and the Manakov system [46]. Compared to the scalar SRB, there are two individual eigenvalues corresponding to two different wave modes consisting of the vector SRBs. As a result, the vector SRBs formed by the nonlinear superposition of two quasi-ABs in the Manakov system are a kind of higher-order nondegenerate breather absent in the standard NLSE. This methodology allows for the derivation of exact relation between MI growth rate and the velocity difference linked to the two eigenvalues, rather than a set of symmetrical spectral parameters [46].

Nevertheless, the dynamics of vector SRBs in the presence of higher-order effects remains an open issue that needs to be further addressed. These effects, which not only produce compression phenomena in breathers and RWs [47,48] but, more importantly, precipitate state transitions [40], demand a profound exploration of their impacts on vector SRBs, particularly as such phenomena are absent in scalar systems. The coupled Hirota (CH) equations were first proposed by Tasgal and Potasek to describe a nonrelativistic boson field [49], which can more accurately describe localized waves in nonlinear systems such as microstructured optical fibers and fiber lasers [50,51]. These equations read as

$$i\psi_t^{(j)} + \tfrac{1}{2}\psi_{xx}^{(j)} + (|\psi^{(1)}|^2 + |\psi^{(2)}|^2)\psi^{(j)} + i\epsilon Q_j = 0, \quad j = 1, 2, \tag{1}$$

where

$$Q_j = \psi_{xxx}^{(j)} + 3(|\psi^{(1)}|^2 + |\psi^{(2)}|^2)\psi_x^{(j)} + 3\left(\psi^{(1)*}\psi_x^{(1)} + \psi^{(2)*}\psi_x^{(2)}\right)\psi^{(j)}, \tag{2}$$

with $\psi^{(j)}(x,t)$ $(j = 1, 2)$ being two nonlinearly coupled components of the vector wave fields. The physical meaning of the independent variables x and t depends on the particular physical problem of interest. For example, t is commonly a normalized distance along the fiber while x is time in a frame moving with group velocity [52] in optics. In the realm of Bose-Einstein condensates (BECs) or a condensate in quantum liquids, t is time and x is the spatial coordinate [53]. Such equations comprise a linear term accounting for the group velocity dispersion (GVD) and two nonlinear terms pertaining to the self-phase modulation (SPM) and cross-phase modulation (XPM). The final two terms in Q_j, accompanied by a real coefficient ϵ, are responsible for the third-order dispersion (TOD) and a time-delay correction to the cubic term, respectively. The intriguing dark and composite RW dynamics [54] in Eqs. (1) have been elucidated. Additionally, the underlying RWs and its intricate association with MI are disclosed [55]. This insight highlights that, owing to the influence of higher-order effects, the dynamics characterized by Eqs. (1) show unprecedented dynamical behaviors that differ from those observed in the Manakov system. Thus, this inspires us that such a mechanism may give rise to some novel properties of vector SRB solutions, particularly in the context of a nondegenerate case.

In this paper, we will confirm the existence of vector SRBs composed of two individual nondegenerate quasi-ABs in Eqs. (1). We proceed to explore the effects of the higher-order terms on the linear and nonlinear stages of MI described by the vector SRBs, particularly focusing on the excitation of diverse wave modes during the nonlinear stage. Remarkably, the presence of higher-order effects can not only delay the time of the linear MI stage, but also eliminate the absolute difference in group velocities, giving rise to a coherent mode unprecedented in previous scalar equations or the Manakov system. The exact link between the MI growth rate and SRBs induced by the higher-order effects will also be refined. Instead of ignoring the higher-order expansion of the parameter γ, we use four different eigenvalues to reveal this correspondence. This formula gives a more comprehensive explanation of the intrinsic relationship between the growth rate of initial localized perturbation during the linear stage and vector

nondegenerate SRBs. The case of scalar SRBs within the Hirota equation framework is discussed in order to illustrate the fact that vector SRBs are formed by two individual nondegenerate fundamental breathers. However, such nondegenerate solutions are absent in the scalar systems. Our results are confirmed by numerical simulations.

The paper is organized as follows. Exact expressions of the nondegenerate solutions describing the vector SRBs dynamics will be given in Sec. II. The higher-order effects on MI during both linear and nonlinear stages, described by the vector SRBs, will be further explored in Sec. III. Section IV will establish an exact link between the MI growth rate and vector SRBs induced by the higher-order effects. The case of scalar SRBs will be discussed in Sec. V, while Sec. VI will present numerical simulations. Section VII will summarize our conclusions.

II. FUNDAMENTAL SOLUTIONS FOR THE VECTOR SRBs

In this section, we will present the fundamental and second-order SRBs for Eqs. (1) in the nondegenerate context. The exact expressions of the fundamental solutions for SRBs in the Manakov system have been outlined in Ref. [46]. Here, we adopt an analogous technique to produce the exact expressions for the vector SRB solutions with higher-order terms.

By using the Darboux transformation (DT) [56], the explicit expressions of the fundamental breather solutions for Eqs. (1) can be given as

$$\psi^{(j)}_{\mathrm{GB}[1]} = \psi^{(j)}_0\big[1-(1-H)\psi^{(j)}_{gb}\big], \quad j=1,2, \tag{3}$$

where

$$\psi^{(j)}_0 = \exp\left\{ i\beta_j x + i\Big[a_1^2+a_2^2-\frac{\beta_j^2}{2}+\epsilon\big(\beta_j^3-3\big(a_1^2+a_2^2\big)\beta_j - 3a_j^2(\beta_1+\beta_2)\big)\Big]t\right\}$$

are the background vector plane waves of Eqs. (1) with a_j and β_j being the plane wave amplitudes and wave numbers, respectively (see Appendix A: Vector breather solutions via DT). Moreover, H in Eqs. (3) is expressed as

$$H = \sum_{j=1}^{2} \frac{a_j^2}{(\boldsymbol{\chi}+\beta_j)(\boldsymbol{\chi}^*+\beta_j)}, \tag{4}$$

where $\boldsymbol{\chi}$ is the eigenvalue that obeys the relation

$$1+\sum_{j=1}^{2}\frac{a_j^2}{(\boldsymbol{\chi}+\beta_j)(\boldsymbol{\chi}'+\beta_j)}=0, \tag{5}$$

and $\boldsymbol{\chi}'=\boldsymbol{\chi}+\omega+i\alpha$ with α,ω being two real parameters. The pivotal parts of the breather solutions (3) are represented as

$$\psi^{(j)}_{gb} = 2i\boldsymbol{\chi}_i\frac{\mathcal{B}^{(j)}(\boldsymbol{\chi})(e^{\boldsymbol{\Gamma}}+e^{-i\boldsymbol{\Omega}})+\mathcal{B}^{(j)}(\boldsymbol{\chi}')(e^{-\boldsymbol{\Gamma}}+e^{i\boldsymbol{\Omega}})}{\varepsilon(\boldsymbol{\chi})e^{\boldsymbol{\Gamma}}+\varepsilon(\boldsymbol{\chi}')e^{-\boldsymbol{\Gamma}}+\mathcal{D}e^{i\boldsymbol{\Omega}}+\mathcal{D}^*e^{-i\boldsymbol{\Omega}}}, \tag{6}$$

where

$$\mathcal{B}^{(j)}(\cdot)=\frac{1}{\cdot+\beta_j},$$
$$\varepsilon(\cdot)=1+\sum_{j=1}^{2}\frac{a_j^2}{(\cdot+\beta_j)(\cdot^*+\beta_j)},$$
$$\mathcal{D}=1+\sum_{j=1}^{2}\frac{a_j^2}{(\boldsymbol{\chi}'+\beta_j)(\boldsymbol{\chi}^*+\beta_j)}. \tag{7}$$

Other parameters are

$$\boldsymbol{\Gamma}=\alpha[\boldsymbol{x}-V_g(\boldsymbol{\chi},\boldsymbol{\chi}')\boldsymbol{t}], \quad \boldsymbol{\Omega}=\omega[\boldsymbol{x}-V_p(\boldsymbol{\chi},\boldsymbol{\chi}')\boldsymbol{t}], \tag{8}$$

where $\boldsymbol{x}=x-x_{01}$ and $\boldsymbol{t}=t-t_{01}$ with x_{01} and t_{01} being responsible for the spatial and temporal position of the general nondegenerate breather. Here, $V_g(\boldsymbol{\chi},\boldsymbol{\chi}')$ and $V_p(\boldsymbol{\chi},\boldsymbol{\chi}')$ respectively describe the group and phase velocities

$$V_g(\boldsymbol{\chi},\boldsymbol{\chi}')=\frac{1}{\alpha}\Big\{\epsilon\Big[\frac{3}{2}\omega(\boldsymbol{\chi}+\boldsymbol{\chi}')_r(\boldsymbol{\chi}+\boldsymbol{\chi}')_i+\frac{3}{4}\alpha(\boldsymbol{\chi}+\boldsymbol{\chi}')_r^2 - \frac{3}{4}\alpha(\boldsymbol{\chi}+\boldsymbol{\chi}')_i^2-\alpha\Big(\frac{9}{4}\omega^2+\frac{1}{4}\alpha^2+2\boldsymbol{a}^2\Big)\Big] + \frac{\alpha}{2}(\boldsymbol{\chi}+\boldsymbol{\chi}')_r+\frac{\omega}{2}(\boldsymbol{\chi}+\boldsymbol{\chi}')_i\Big\} \tag{9}$$

and

$$V_p(\boldsymbol{\chi},\boldsymbol{\chi}')=\frac{1}{\omega}\Big\{\epsilon\Big[\frac{3}{4}\omega(\boldsymbol{\chi}+\boldsymbol{\chi}')_r^2-\frac{3}{4}\omega(\boldsymbol{\chi}+\boldsymbol{\chi}')_i^2-\frac{3}{2}(\boldsymbol{\chi}+\boldsymbol{\chi}')_r \times(\boldsymbol{\chi}+\boldsymbol{\chi}')_i+\omega\Big(\frac{\omega^2}{4}-\frac{3\alpha^2}{4}-2\boldsymbol{a}^2\Big)-\boldsymbol{a}^2\Big] + \frac{\omega}{2}(\boldsymbol{\chi}+\boldsymbol{\chi}')_r-\frac{\alpha}{2}(\boldsymbol{\chi}+\boldsymbol{\chi}')_i\Big\}, \tag{10}$$

with $\boldsymbol{a}^2=a_1^2+a_2^2$.

When the value of the parameter α is very small but nonzero, Eqs. (3) describe the vector quasi-ABs with finite envelope width $1/\alpha$. The vector SRBs can be formed by the nonlinear superposition of a pair of quasi-ABs, and each of them has a finite period $2\pi/\omega$ and the width $1/\alpha$, and the exact expressions of $\psi^{(j)}_{\mathrm{SRB}}(x,t)$ $(j=1,2)$ are presented in Appendix B: Higher-order breather solutions via DT. However, the vector SRBs cannot be formed by two arbitrary fundamental quasi-ABs since they must be in the nondegenerate context. From Eqs. (6), (9), and (10), the physical properties of quasi-ABs are mainly determined by their eigenvalues. The expressions of possible eigenvalues are obtained from Eq. (5):

$$\begin{aligned}
\boldsymbol{\chi}_1&=-\frac{\omega}{2}-\frac{i\alpha}{2}-\sqrt{\mu-\sqrt{\nu}},\\
\boldsymbol{\chi}_2&=-\frac{\omega}{2}-\frac{i\alpha}{2}+\sqrt{\mu-\sqrt{\nu}},\\
\boldsymbol{\chi}_3&=-\frac{\omega}{2}-\frac{i\alpha}{2}-\sqrt{\mu+\sqrt{\nu}},\\
\boldsymbol{\chi}_4&=-\frac{\omega}{2}-\frac{i\alpha}{2}+\sqrt{\mu+\sqrt{\nu}},
\end{aligned} \tag{11}$$

with

$$\mu = \beta^2 - a^2 + \frac{(\omega + i\alpha)^2}{4}, \quad \nu = a^4 - 4a^2\beta^2 + (\omega + i\alpha)^2\beta^2. \tag{12}$$

Therefore, the formation of vector SRBs is subject to the existence of specific nondegenerate quasi-ABs that are associated with two distinct eigenvalues. Further analysis shows that the eigenvalues χ_k $(k = 1, 2, 3, 4)$ satisfy certain symmetric properties

$$\begin{aligned} \chi_{1r} + \chi_{2r} &= \chi'_{1r} + \chi'_{2r} = -\omega, \\ \chi_{1i} + \chi_{2i} &= \chi'_{1i} + \chi'_{2i} = -\alpha, \\ \chi_{3r} + \chi_{4r} &= \chi'_{3r} + \chi'_{4r} = -\omega, \\ \chi_{3i} + \chi_{4i} &= \chi'_{3i} + \chi'_{4i} = -\alpha, \end{aligned} \tag{13}$$

and

$$\begin{aligned} \chi_{1r} + \chi'_{1r} &= -(\chi_{2r} + \chi'_{2r}), \\ \chi_{1i} + \chi'_{1i} &= -(\chi_{2i} + \chi'_{2i}), \\ \chi_{3r} + \chi'_{3r} &= -(\chi_{4r} + \chi'_{4r}), \\ \chi_{3i} + \chi'_{3i} &= -(\chi_{4i} + \chi'_{4i}), \end{aligned} \tag{14}$$

where the subscripts r and i denote the real and imaginary parts, respectively. As a result, the group and phase velocities corresponding to four different eigenvalues satisfy the following relations:

$$\begin{aligned} V_g(\chi_1, \chi'_1) - V_g(\chi_2, \chi'_2) &= \alpha(\chi_1 + \chi'_1)_r + \omega(\chi_1 + \chi'_1)_i, \\ V_p(\chi_1, \chi'_1) - V_p(\chi_2, \chi'_2) &= \omega(\chi_1 + \chi'_1)_r - \alpha(\chi_1 + \chi'_1)_i, \\ V_g(\chi_3, \chi'_3) - V_g(\chi_4, \chi'_4) &= \alpha(\chi_1 + \chi'_1)_r + \omega(\chi_1 + \chi'_1)_i, \\ V_p(\chi_3, \chi'_3) - V_p(\chi_4, \chi'_4) &= \omega(\chi_1 + \chi'_1)_r - \alpha(\chi_1 + \chi'_1)_i. \end{aligned} \tag{15}$$

From the above results, one can easily observe that the group velocities of $\psi^{(j)}_{\mathrm{GB}[1]}(\chi_1, \chi'_1)$ [or $\psi^{(j)}_{\mathrm{GB}[1]}(\chi_3, \chi'_3)$] are symmetric with $\psi^{(j)}_{\mathrm{GB}[1]}(\chi_2, \chi'_2)$ [or $\psi^{(j)}_{\mathrm{GB}[1]}(\chi_4, \chi'_4)$] along a certain direction in the CH equations (1). Although the direction of such symmetric axis can be affected by the higher-order effects, the absolute difference of two group velocities does not depend on the higher-order coefficient ϵ. Besides, the nonlinear superposition of two fundamental breathers $\psi^{(j)}_{\mathrm{GB}[1]}(\chi_1, \chi'_1)$ and $\psi^{(j)}_{\mathrm{GB}[1]}(\chi_2, \chi'_2)$ [or, alternatively, $\psi^{(j)}_{\mathrm{GB}[1]}(\chi_3, \chi'_3)$ and $\psi^{(j)}_{\mathrm{GB}[1]}(\chi_4, \chi'_4)$] cannot form the vector SRBs. In other words, the formation of SRBs fully depends on two individual quasi-ABs with two different pairs of eigenvalues χ_1, χ'_1 and χ_3, χ'_3 (or, alternatively, χ_2, χ'_2 and χ_4, χ'_4). The above properties are very different from those in the Manakov system. Specifically speaking, when $\epsilon = 0$, the symmetric axis of two group velocities corresponding to χ_1, χ'_1 and χ_2, χ'_2 (or, alternatively, χ_3, χ'_3 and χ_4, χ'_4) is the t axis. It means that the above two quasi-ABs have opposite group velocities. Such symmetric properties will disappear in the CH equations (1) due to the higher-order effects. However, the symmetric axis about $\psi^{(j)}_{\mathrm{GB}[1]}(\chi_1, \chi'_1)$, $\psi^{(j)}_{\mathrm{GB}[1]}(\chi_2, \chi'_2)$ and the symmetric axis about $\psi^{(j)}_{\mathrm{GB}[1]}(\chi_3, \chi'_3)$, $\psi^{(j)}_{\mathrm{GB}[1]}(\chi_4, \chi'_4)$ have opposite directions in the CH equations (1).

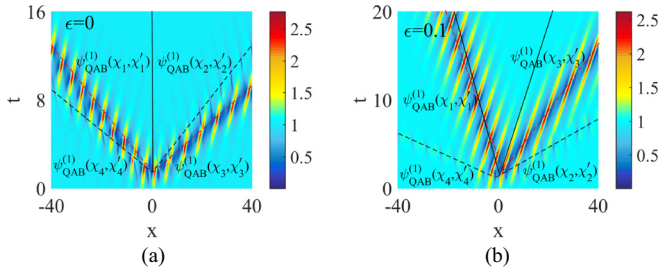

FIG. 1. Amplitude profiles for the first wave component of the second-order vector SRBs in (a) the Manakov system ($\epsilon = 0$) and (b) the CH equations ($\epsilon = 0.1$). The dark and red dashes in each panel indicate the fundamental quasi-ABs involved in the SRBs. The dark solid lines are symmetric axes of $\psi^{(1)}_{\mathrm{QAB}}(\chi_1, \chi'_1)$, $\psi^{(1)}_{\mathrm{QAB}}(\chi_2, \chi'_2)$ and $\psi^{(1)}_{\mathrm{QAB}}(\chi_3, \chi'_3)$, $\psi^{(1)}_{\mathrm{QAB}}(\chi_4, \chi'_4)$, respectively. The parameters are $a = 1, \alpha = 0.2, \omega = 1.2, \beta = 1$.

Figure 1 shows the amplitude profiles of the first wave component of second-order SRBs $\psi^{(1)}_{\mathrm{SRB}[2]}$ formed by four individual quasi-ABs in the Manakov system and the CH equations As shown in Fig. 1, there is merely one symmetric axis for four fundamental breathers in the Manakov system, while there are two different axes in the presence of the higher-order effects. It is also worthwhile to notice that two such axes in Eqs. (1) are symmetric with the t axis. Figure 2 displays the amplitude profiles of vector SRBs formed by

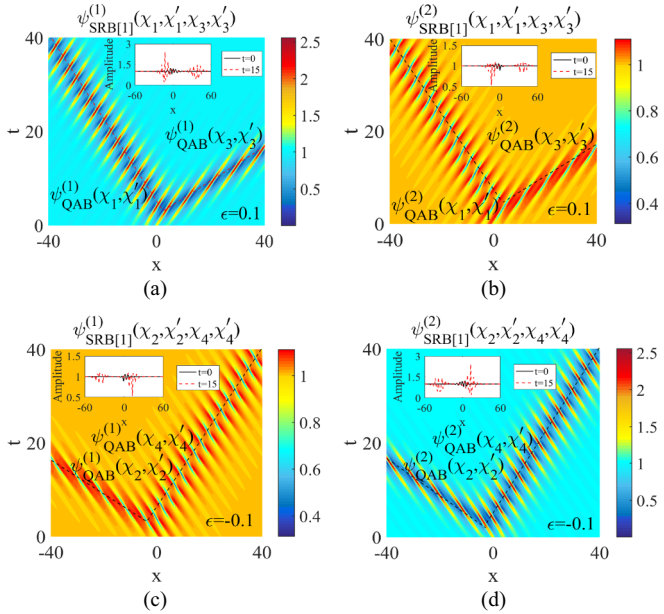

FIG. 2. Amplitude profiles of two components $\psi^{(j)}_{\mathrm{SRB}[1]}(\chi_{[1]}, \chi'_{[1]}, \chi_{[2]}, \chi'_{[2]})$ $(j = 1, 2)$. The real parameters are $a = 1, \alpha = 0.2, \omega = 1.2, \beta = 1, \epsilon = \pm 0.1$. (a) The amplitude of the first component with $\chi_{[1]} = \chi_1, \chi_{[2]} = \chi_3$. (b) The amplitude of the second component with $\chi_{[1]} = \chi_1, \chi_{[2]} = \chi_3$. (c) The amplitude of the first component with $\chi_{[1]} = \chi_2, \chi_{[2]} = \chi_4$. (d) The amplitude of the second component with $\chi_{[1]} = \chi_2, \chi_{[2]} = \chi_4$. The small inset in each panel shows the amplitude of SRBs at $t = 0$ and $t > 0$ and two dark dashes indicate the velocities of two quasi-ABs composing the SRBs. The small inset in each panel shows the amplitude profiles of SRBs at $t = 0$ and $t = 10$, respectively.

two different quasi-ABs corresponding to two individual pairs of eigenvalues χ_1, χ_1' (or χ_2, χ_2') and χ_3, χ_3' (or χ_4, χ_4'). It indicates that the SRBs are formed by two quasi-ABs sharing identical structural characteristics but different group velocities. Further, the insets in Fig. 2 show an initial small localized perturbation, which subsequently propagates along two distinct directions, undergoing a transformation into oscillatory structures characterized by the amplified amplitudes.

In scalar NLSE, the SRB exemplifies a breather solution, offering a theoretical framework for describing the nonlinear evolution of MI developing from a small localized perturbation [8]. The solution is obtained via the dressing method and the Jukowsky transformation [24], characterized by two symmetric spectral parameters. However, in the coupled nonlinear systems, the vector SRBs exhibit a distinct signature, comprising four individual eigenvalues that correspond to four independent wave modes. Therefore, the vector SRBs are classified as nondegenerate breathers, a phenomenon absent in the scalar systems. Although such solutions have been studied in Ref. [46], those encountered in Eqs. (1), incorporating higher-order terms, may exhibit novel dynamic behaviors. These unique attributes cannot be observed in the vector SRBs of the Manakov system. We will delve into a detailed discussion in the next section.

III. MI INDUCED BY HIGHER-ORDER EFFECTS

In this section, we will explore the higher-order effects on the MI described by the vector SRBs in Eqs. (1). Since the evolution of MI described by the fundamental vector SRBs involves two distinct processes, namely linear and nonlinear stages, we proceed to investigate the effects on each of these stages.

A. Linear stage

In this subsection, we will elaborate on the influence of higher-order effects on the velocity difference of two nondegenerate quasi-ABs that constitute the vector SRBs for Eqs. (1). Moreover, we will also provide the higher-order effects on the MI growth rate in the linear stage.

We study the SRBs $\psi^{(j)}_{\mathrm{SRB}[1]}(\chi_1, \chi_1', \chi_3, \chi_3')$ $(j = 1, 2)$ and $\psi^{(j)}_{\mathrm{SRB}[1]}(\chi_2, \chi_2', \chi_4, \chi_4')$ $(j = 1, 2)$. Two different eigenvalues in the vector SRBs correspond to two individual quasi-ABs, and their velocity difference can be expressed as

$$\Delta V_g(\chi_{[1]}, \chi_{[1]}', \chi_{[2]}, \chi_{[2]}') = \Delta V_1(\chi_{[1]}, \chi_{[1]}', \chi_{[2]}, \chi_{[2]}') + \epsilon \Delta V_2(\chi_{[1]}, \chi_{[1]}', \chi_{[2]}, \chi_{[2]}'), \tag{16}$$

with

$$\Delta V_1(\chi_{[1]}, \chi_{[1]}', \chi_{[2]}, \chi_{[2]}') = \frac{\alpha}{2}[(\chi_{[1]} + \chi_{[1]}')_r - (\chi_{[2]} + \chi_{[2]}')_r] + \frac{\omega}{2}[(\chi_{[1]} + \chi_{[1]}')_i - (\chi_{[2]} + \chi_{[2]}')_i], \tag{17}$$

$$\Delta V_2(\chi_{[1]}, \chi_{[1]}', \chi_{[2]}, \chi_{[2]}') = \frac{3\omega}{2}[(\chi_{[1]} + \chi_{[1]}')_r(\chi_{[1]} + \chi_{[1]}')_i - (\chi_{[2]} + \chi_{[2]}')_r(\chi_{[2]} + \chi_{[2]}')_i] + \frac{3\alpha}{4}\big[(\chi_{[1]} + \chi_{[1]}')_r^2 + (\chi_{[2]} + \chi_{[2]}')_i^2 - (\chi_{[2]} + \chi_{[2]}')_r^2 - (\chi_{[1]} + \chi_{[1]}')_i^2\big]. \tag{18}$$

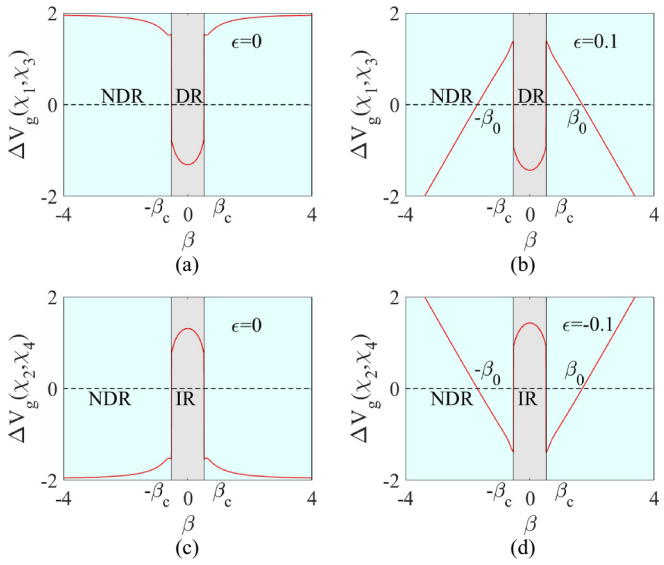

FIG. 3. The velocity difference of two different quasi-ABs corresponding to two pairs of individual eigenvalues (a) χ_1, χ_1' and χ_3, χ_3' with $\epsilon = 0$, (b) χ_1, χ_1' and χ_3, χ_3' with $\epsilon = 0.1$, (c) χ_2, χ_2' and χ_4, χ_4' with $\epsilon = 0$, (d) χ_2, χ_2' and χ_4, χ_4' with $\epsilon = -0.1$. Two vertical dark lines in each panel represent the region of relative wave number β_c. In two cyan regions outside of the dark lines, the value of β corresponds to the nondegenerate solutions and the short form "NDR" represents "nondegenerate region." When $\epsilon \neq 0$, the velocity difference will be zero at points of $\beta = \pm\beta_0$. On the other hand, for the solutions with eigenvalues χ_1, χ_1' and χ_3, χ_3', the gray area within two solid dark lines corresponds to the region of degenerate solutions. However, there are no solutions in the gray area when the eigenvalues are taken to be χ_2, χ_2' and χ_4, χ_4'. The short forms "DR" and "IR" stand for "degenerate region" and "invalid region," respectively.

Here, $\chi_{[1]} = \chi_1$ (or χ_2) and $\chi_{[2]} = \chi_3$ (or χ_4).

From the above expressions, the item $\Delta V_1(\chi_{[1]}, \chi_{[1]}', \chi_{[2]}, \chi_{[2]}')$ in the velocity difference always exists, while $\Delta V_2(\chi_{[1]}, \chi_{[1]}', \chi_{[2]}, \chi_{[2]}')$ will disappear when $\epsilon = 0$. This indicates that adding the higher-order effects will produce a significant influence on the velocity difference. Based on its relationship to MI growth rate, this effect can further affect the growth dynamics of initial localized perturbation during the linear stage. In the case of such condition, the velocity difference will not be equal to zero for an arbitrary set of parameters, as shown in Fig. 3(a). However, when $\epsilon \neq 0$, the value of velocity difference of two quasi-ABs corresponding to two pairs of eigenvalues $\chi_{[1]}, \chi_{[1]}'$ and $\chi_{[2]}, \chi_{[2]}'$ can be zero at two certain points with $\beta = \pm\beta_0$, which is depicted in Figs. 3(b) and 3(d). Furthermore, the absolute value of the velocity difference decreases before the relative wave number β reaches the point $\pm\beta_0$ while it increases after reaching the two points. In order to further study the higher-order effects on the absolute difference of the group velocities, we describe the relation between velocity difference and higher-order coefficient ϵ in Fig. 4.

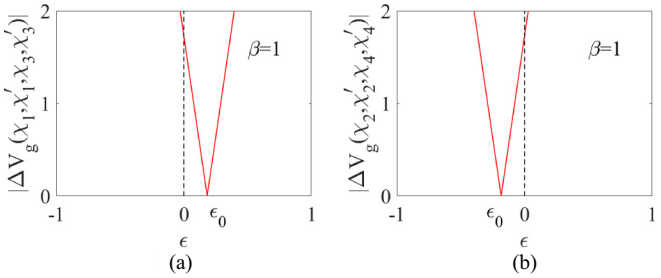

FIG. 4. The absolute difference of the group velocities with the higher-order coefficient ϵ. The relative wave number is $\beta = 1$ and other parameters are similar to those in Fig. 2.

One can obviously find that there exists a special point ϵ_0 in each panel of the figure. At such point, the absolute velocity difference becomes zero. In this way, only if $\epsilon = \epsilon_0$, the SRBs propagate along a certain direction just as shown in Fig. 6(a). The exact link between MI and the absolute difference of two group velocities of the scalar SRB has been discovered in several integrable systems, including the NLSE [41], the complex modified KdV equation [34], the NLS-MB equation [45], and the Manakov system [46], to name a few. However, the nondegenerate solutions are generally absent in scalar systems. In addition, due to the influence of the higher-order effects, the perspectives of vector SRBs are much different from those in the Manakov system. Specifically speaking, two group velocities of SRBs can never be equal without higher-order effects. On the other hand, the group velocity difference is closely associated with the MI growth rate in the linear stage (further analysis will be presented in next section). As a result, the higher-order terms will have significant impacts on MI described by the vector SRBs during the linear stage.

From our analysis in the above context, it can be concluded that the change of absolute value for the velocity difference can affect the propagation characteristics of the vector SRBs. Despite the expression of velocity difference being decided by the relative wave number β, the higher-order coefficient ϵ

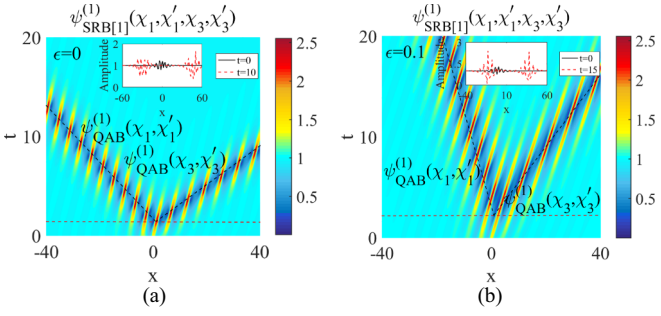

FIG. 5. Amplitude profiles of the first wave component for the fundamental SRBs $\psi^{(1)}_{\mathrm{SRB}[1]}(\chi_1, \chi_1', \chi_3, \chi_3')$ with higher-order coefficient being different values (a) $\epsilon = 0$ and (b) $\epsilon = 0.1$. Other parameters are similar to those in Fig. 2. Red dashes in each panel serve to delineate the linear and nonlinear stages in the evolution while dark solid lines represent the propagation directions of two quasi-ABs contained in the SRBs. The small inset in each panel shows the amplitude profiles of the SRBs at $t = 0$ and $t \neq 0$, respectively.

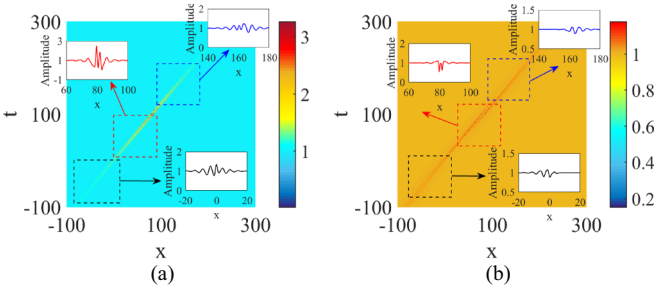

FIG. 6. Amplitude profiles of two wave components for the fundamental SRBs (a) $\psi^{(1)}_{\mathrm{SRB}[1]}(\chi_1, \chi_1', \chi_3, \chi_3')$ and (b) $\psi^{(2)}_{\mathrm{SRB}[1]}(\chi_1, \chi_1', \chi_3, \chi_3')$. The higher-order coefficient is $\epsilon = \epsilon_0$, at which point two group velocities in SRBs are equal. Other parameters are similar to those in Fig. 5. Three insets in each panel are the profile maps at $t = 0$, $t = 100$, and $t = 200$.

as well as the real parameters α and ω, we mainly consider the effects of higher-order terms on the SRBs owing to their physical significance. By choosing different values of the parameters ϵ, we show such effects on the solutions during the linear stage. We here take the first wave component of vector SRB solution $\psi^{(1)}_{\mathrm{SRB}[1]}(\chi_1, \chi_1', \chi_3, \chi_3')$ as an example.

Figure 5 shows the amplitude profile of the first wave component with different values of the higher-order coefficient. One can clearly observe that the evolution of localized perturbation in the initial stage is prolonged with the increase of the values of ϵ before reaching ϵ_0. This finding once again validates the relation between velocity difference and the MI growth rate proposed in the complex modified KdV equation [34]. In contrast to Ref. [34], where the change in velocity difference are not attributed to the changes in higher-order terms, our results originate precisely from such adjustments. Thus, we can regulate the evolution dynamics of localized small perturbations during the initial stage by adjusting the values of higher-order terms.

When $\epsilon = \epsilon_0$, the small multipeak localized perturbation neither evolves into two quasi-ABs nor is completely suppressed. In the previous study within the NLSE hierarchy framework [34], a small-amplitude perturbation evolves along a certain direction with small oscillations, while the amplification of the perturbation is suppressed completely. This SRB pattern physically represents a nonamplifying propagation of wave dynamics, which corresponds to a zero growth rate of MI [34]. However, as discussed above, such mode does not exist in the Manakov system. But incorporating higher-order terms (the CH equations) into such equations may result in different outcomes. As we expected, a novel bound state of SRBs is shown in Fig. 6 clearly. This beating pattern can be attributed to the equivalence of the two group velocities in the vector SRB waves, which is induced by the higher-order effects. In this scenario, two quasi-ABs residing within the SRBs show coherent interaction. Within an oscillatory cycle, three distinct stages can be identified, corresponding to the three dotted box regions exhibited in Fig. 6. In the first stage, the small localized perturbation experiences negligible amplitude growth, undergoing a prolonged period of nongrowing evolution until it transitions into the second stage. During this second stage, the amplitude is rapidly amplified, followed by

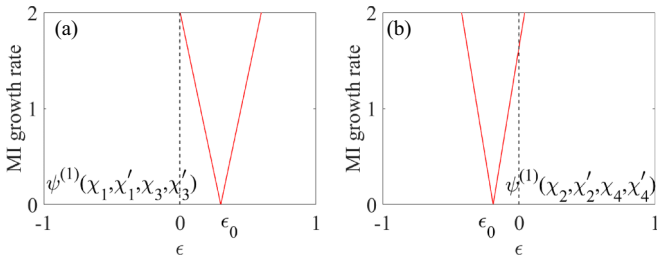

FIG. 7. MI growth rate $\mathcal{G}$ (19) of the fundamental SRBs (a) $\psi^{(1)}_{\mathrm{SRB}[1]}(\chi_1, \chi_1', \chi_3, \chi_3')$ and (b) $\psi^{(1)}_{\mathrm{SRB}[1]}(\chi_2, \chi_2', \chi_4, \chi_4')$ under higher-order effects. Other parameters are $a = 1, \omega = 1.2, \alpha = 0.2, \beta = 1$.

a subsequent attenuation. In the third stage, the amplitude of this bound state returns to the level comparable to the initial small localized perturbation. It is very worthwhile to note that the amplitude profiles shown in Fig. 6 are fundamentally different from the NLSE described in Ref. [34]. The small localized perturbation in Fig. 6 will grow and then decay after a long period of time. The physical explanation behind this phenomenon remains unclear and may be related to the nondegenerate characteristic of the solutions. This result can be used for the study of SRB bound states in specially designed optical systems described by the higher-order NLSEs with fixed structural parameters.

Then we further study the mechanism of MI growth rate varying with the higher-order terms. More details on the exact expression of MI growth rate will be given in Sec. IV. Here we merely use the results of MI growth rate for Eqs. (1) [57],

$$\mathcal{G} = \mathrm{Im}[18\epsilon a^2 - 6\epsilon\beta^2 - 2\epsilon Q^2 \pm 6\epsilon\sqrt{a^4 - 4a^2\beta^2 + \beta^2 Q^2} \pm \sqrt{4\beta^2 - 4a^2 + Q^2 \mp 4\sqrt{a^4 - 4a^2\beta^2 + \beta^2 Q^2}}]. \quad (19)$$

Figure 7 shows the MI growth rate with the change of higher-order coefficient ϵ. One can find that the MI growth rate becomes zero at a certain point ϵ_0 of each panel. The aforementioned result can be mutually corroborated with the finding presented in Fig. 4 regarding the relationship between the velocity difference and higher-order term ϵ. Later, we will explore the precise relationship between the vector SRB and MI growth rate based on this formula.

B. Nonlinear stage

In this subsection, we will investigate the characteristics of nonlinear stage of MI developed from the localized multipeak weak perturbations, namely the nonlinear excitations of different types of nondegenerate wave modes for the vector SRBs.

In fact, previous studies have already delved into this issue, primarily focusing on the SRB mechanism in scalar systems, or the SRB dynamics in vector systems without higher-order effects. The Lakshmanan-Porsezian-Daniel equation with the fourth dispersive and nonlinear terms has emerged as a primary focus of concern [40]. It is found that a fascinating dynamic where a small localized perturbation can evolve into three different types of states during the nonlinear stages of MI, including the coexistence of a quasi-AB and a multipeak soliton, the formation of two stable multipeak solitons moving in opposite directions, and a pulsating structure formed by two stable multipeak solitons moving in the same direction. Importantly, these patterns are not observed in the standard NLSE, indicating that they are unique characteristics induced by higher-order effects. Further findings into the complex modified KdV equation [34] have revealed some novel intriguing dynamics. In particular, the half-transition mode exhibits a unique mixed pattern with a quasi-AB and quasiperiodic waves, while the full-suppression mode shows a distinct nonamplifying behavior characterized by localized small perturbations linked to the diminishing growth rate of MI. Remarkably, both analytical and numerical analyses confirm that these distinct SRBs can originate from an identical small localized perturbation, highlighting a profound relation between SR modes and the outcomes of linear stability analysis. Moreover, Liu *et al.* discovered a novel type of interference patterns emerging from the focusing NLSE with localized periodic initial conditions. These patterns exhibit distinctive chess-board-like spatiotemporal structures, observable as a direct outcome of the collision between two breathers [13]. A significant advancement has been achieved in the analysis of vector systems. Liu *et al.* successfully formulated an exact theory describing the behavior of vector SRBs within the framework of the Manakov equations [46]. Notably, in the context of nondegenerate solutions, the existence of these vector SRBs has been verified in both the focusing and defocusing Manakov systems. This comprehensive theory relies heavily on a detailed eigenvalue analysis, further revealing the exact relation between SRBs and MI. A noteworthy finding is that, under focusing conditions, a localized periodic initial modulation of the plane wave has the potential to trigger not just a single SRB, but also more intricate second-order SRBs. The aforementioned research work has further developed the study of the nonlinear stage of MI. However, within the framework of vector SRBs, the characteristics of the nonlinear stage of MI considering higher-order effects have yet to be explored.

In addition to the fundamental nondegenerate SRB waves, one can expect that there are other kinds of wave modes during the nonlinear stage for Eqs. (1) due to the presence of higher-order effects. These effects will significantly reshape the vector SRB waves, introducing complexities and variations that deviate from the fundamental modes. This suggests that a small localized perturbation can evolve into a richer variety of modes distinct from the fundamental mode during the nonlinear stage of MI. The related studies have primarily been conducted in the context of scalar SRBs [40,41]; however, the mechanism remains an unresolved issue for the vector ones. From Eqs. (9) and (10), one can observe that the group and phase velocities are closely related to the excitations of wave mode of the vector SRB solutions $\psi^{(j)}_{\mathrm{SRB}[1]}(\chi_{[1]}, \chi'_{[1]}, \chi_{[2]}, \chi'_{[2]})$. Under a specific condition, the coincidence of group and phase velocities of the quasi-ABs embedded within the vector SRBs will trigger a multipeak soliton state. We provide a detailed analytical examination in the following part.

There are two characteristic lines in the quasi-AB, which are expressed as follows:

$$\boldsymbol{L}_p : \alpha x + \Big\{\epsilon\Big[6\omega\boldsymbol{\chi}_i\Big(\boldsymbol{\chi}_r + \frac{\omega}{2}\Big) + 3\alpha(\boldsymbol{\chi}_r + \omega)^2 - \alpha\big(3\boldsymbol{\chi}_i^2 + 3\alpha\boldsymbol{\chi}_i + \alpha^2\big)\Big] + \alpha\boldsymbol{\chi}_r + \omega\boldsymbol{\chi}_i + \omega\alpha - 2\epsilon\alpha\big(a_1^2 + a_2^2\big)\Big\}t = c_1, \tag{20}$$

$$\boldsymbol{L}_s : \omega x + \Big\{\epsilon\omega\Big[\big(3\boldsymbol{\chi}_r^2 + 3\omega\boldsymbol{\chi}_r + \omega^2\big) - 3\Big(2\alpha\boldsymbol{\chi}_r\Big(\boldsymbol{\chi}_i + \frac{\alpha}{2}\Big) + \omega(\boldsymbol{\chi}_i + \alpha)^2\Big)\Big] + \omega\Big(\boldsymbol{\chi}_r + \frac{\omega}{2}\Big) - \alpha\Big(\boldsymbol{\chi}_i + \frac{\alpha}{2}\Big) - 2\epsilon\omega\big(a_1^2 + a_2^2\big) - \epsilon\big(a_1^2 + a_2^2\big)\Big\}t = c_2. \tag{21}$$

Their directions are denoted as $\boldsymbol{D}_p$ and $\boldsymbol{D}_g$, characterizing the properties of solitary-wave component and periodic-wave component respectively. When these two directions are mutually parallel, the quasi-ABs can undergo a transformation into the multipeak solitons. This condition is mathematically formulated as the relation

$$\boldsymbol{V}_g = \boldsymbol{V}_p. \tag{22}$$

The solutions of the quasi-ABs can be rewritten as the nonlinear combination of the trigonometric function $\cos\boldsymbol{\Omega}$ and hyperbolic function $\cosh\boldsymbol{\Gamma}$:

$$\psi_{\mathrm{QAB}}^{(j)} = \rho_j\psi_0^{(j)}\psi_{\mathrm{qab}}^{(j)}, \quad j = 1, 2, \tag{23}$$

where

$$\rho_j = \frac{\boldsymbol{\chi}'^{*} + \beta_j}{\boldsymbol{\chi}' + \beta_j}\sqrt{\frac{(\boldsymbol{\chi}^{*} + \beta_j)(\boldsymbol{\chi}'^{*} + \beta_j)}{(\boldsymbol{\chi} + \beta_j)(\boldsymbol{\chi}' + \beta_j)}} \tag{24}$$

and

$$\psi_{\mathrm{qab}}^{(j)} = \frac{\kappa\cosh(\boldsymbol{\Gamma} + i\delta_j) + \varpi\cos(\boldsymbol{\Omega} + i\gamma_j)}{\kappa\cosh\boldsymbol{\Gamma} + \varpi\cos\boldsymbol{\Omega}}. \tag{25}$$

The above results mean the quasi-ABs can be regarded as the nonlinear superposition of the periodic wave and a solitary wave. When the group velocity is equal to the phase velocity [i.e., satisfying Eq. (22)], both wave components have the same characteristic direction. As a result, the quasi-AB will be transformed into a soliton.

Although there are two sets of group and phase velocities $V_g(\boldsymbol{\chi}_{[1]}, \boldsymbol{\chi}'_{[1]}), V_p(\boldsymbol{\chi}_{[1]}, \boldsymbol{\chi}'_{[1]})$ and $V_g(\boldsymbol{\chi}_{[2]}, \boldsymbol{\chi}'_{[2]}), V_p(\boldsymbol{\chi}_{[2]}, \boldsymbol{\chi}'_{[2]})$ being contained in the SRB solutions $\psi_{\mathrm{SRB}[1]}^{(j)}(\boldsymbol{\chi}_{[1]}, \boldsymbol{\chi}'_{[1]}, \boldsymbol{\chi}_{[2]}, \boldsymbol{\chi}'_{[2]})$ $(j = 1, 2)$, they cannot satisfy the relation (22) simultaneously (see Fig. 8). Thus, only one of the quasi-ABs can be converted into a soliton, as shown in Fig. 9, which presents the transformed SRBs $\psi_{\mathrm{SRB}[1]}^{(j)}(\boldsymbol{\chi}_1, \boldsymbol{\chi}'_1, \boldsymbol{\chi}_3, \boldsymbol{\chi}'_3)$ and $\psi_{\mathrm{SRB}[1]}^{(j)}(\boldsymbol{\chi}_2, \boldsymbol{\chi}'_2, \boldsymbol{\chi}_4, \boldsymbol{\chi}'_4)$, respectively. We can clearly observe that, as time evolves, a small localized perturbation develops into a quasi-AB and a multipeak soliton during the nonlinear stage of MI. In the Manakov system, there is no such analog. As the vector SRBs are composed of two quasi-ABs, the solitary and periodic wave components are inherent and neither of them will disappear alone. As a result,

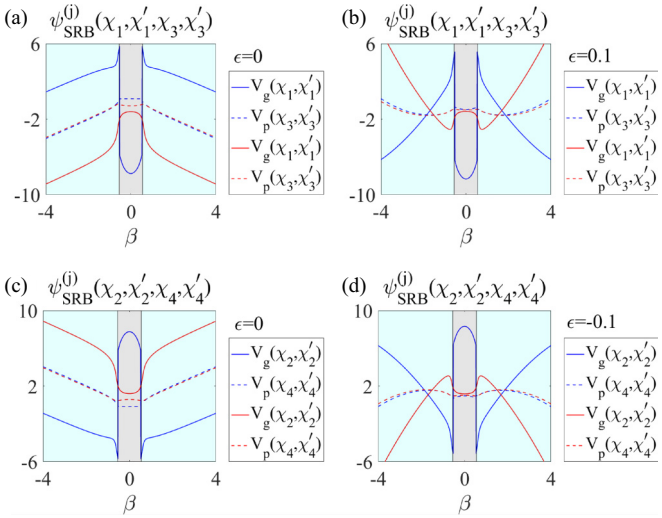

FIG. 8. The group and phase velocities of two quasi-ABs contained in the SRBs $\psi_{\mathrm{SRB}[1]}^{(j)}(\boldsymbol{\chi}_{[1]}, \boldsymbol{\chi}'_{[1]}, \boldsymbol{\chi}_{[2]}, \boldsymbol{\chi}'_{[2]})$, $j = 1, 2$. (a) $\boldsymbol{\chi}_{[1]} = \boldsymbol{\chi}_1, \boldsymbol{\chi}_{[2]} = \boldsymbol{\chi}_3$ and $\epsilon = 0$, (b) $\boldsymbol{\chi}_{[1]} = \boldsymbol{\chi}_1, \boldsymbol{\chi}_{[2]} = \boldsymbol{\chi}_3$ and $\epsilon \neq 0$, (c) $\boldsymbol{\chi}_{[1]} = \boldsymbol{\chi}_2, \boldsymbol{\chi}_{[2]} = \boldsymbol{\chi}_4$ and $\epsilon = 0$, (d) $\boldsymbol{\chi}_{[1]} = \boldsymbol{\chi}_2, \boldsymbol{\chi}_{[2]} = \boldsymbol{\chi}_4$ and $\epsilon \neq 0$. The value of β is valid only if it is in the region of the cyan area (nondegenerate regime) of each panel. Other parameters are similar to those in Fig. 2.

they can only be transformed into multipeak solitons rather than evolving into alternative wave patterns, such as periodic, W-shaped, or M-shaped waves. Based on the preceding analysis, one can conclude that the linear and nonlinear stages of MI, as described by the vector SRBs within the framework of Eqs. (1) incorporating higher-order effects, are very different from those in the Manakov system. More precisely, the higher-order effects can extend the evolution duration of the small localized perturbation during the linear stage when the difference between two group velocities is not equal to zero. Moreover, when the difference vanishes, the evolution time is significantly increased, leading to sustained coherent interactions between two quasi-ABs in their initial perturbed state. On the other hand, the difference between the group and phase velocities is affected by the higher-order effects. When it equals zero, a phase transition occurs in the evolution state of the localized perturbation during the nonlinear stage of MI. As a result, the small localized perturbation in the initial condition may be excited to other types of wave modes. Such results illustrate that one may control the MI characteristics of initial perturbations in both linear and nonlinear stages by adjusting the higher-order coefficient ϵ in such model. Our results offer valuable insights for further exploration of chaotic wave fields and integrable turbulence.

IV. IMPROVED EXACT LINK

In this section, we will further investigate the linear MI described by the vector SRBs in Eqs. (1). The exact links between MI and the absolute difference of two group velocities for the SRBs in the infinite NLSE hierarchy [41] and the Manakov system [46] have been established. By performing Taylor expansion and approximation on the parameter α, the latter involved the utilization of the eigenvalues $\boldsymbol{\chi}_{[1]}$ (and $\boldsymbol{\chi}'_{[1]}$)

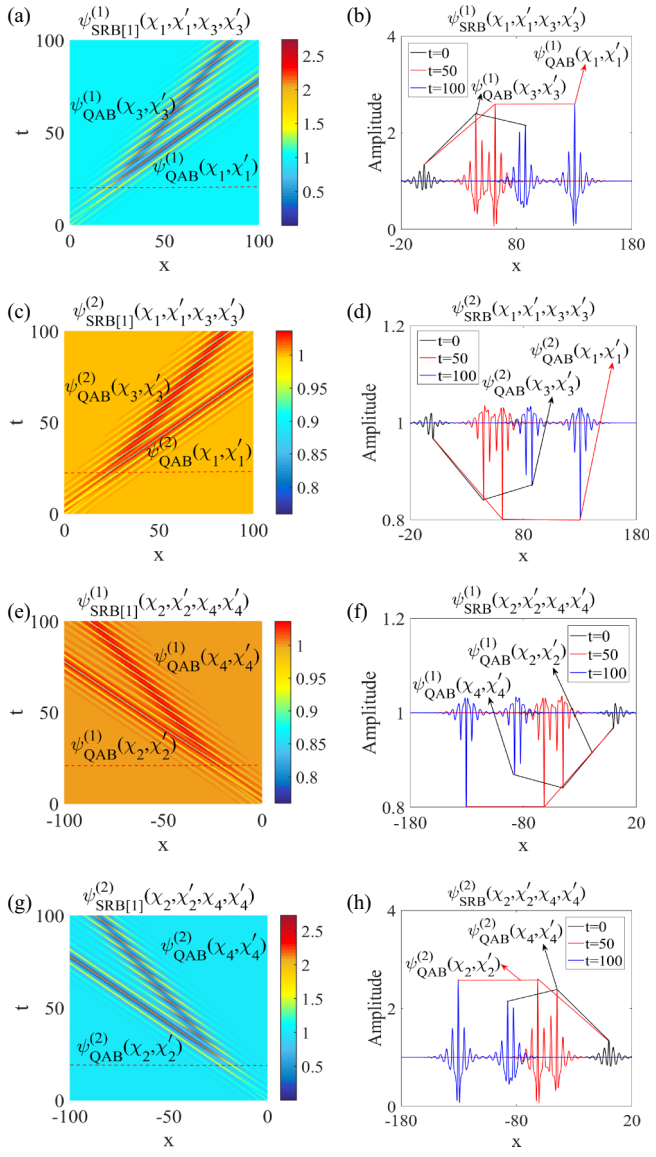

FIG. 9. Amplitude profiles of two components for the SRBs: (a), (c) $\psi^{(j)}_{\mathrm{SRB}[1]}(\chi_1, \chi_1', \chi_3, \chi_3')$ and (e),(g) $\psi^{(j)}_{\mathrm{SRB}[1]}(\chi_2, \chi_2', \chi_4, \chi_4')$; and their sectional views (b),(d) $\psi^{(j)}_{\mathrm{SRB}[1]}(\chi_1, \chi_1', \chi_3, \chi_3')$ and (f), (h) $\psi^{(j)}_{\mathrm{SRB}[1]}(\chi_2, \chi_2', \chi_4, \chi_4')$ at different t. $\psi^{(j)}_{\mathrm{QAB}}(\chi_k, \chi_k')$ $(j = 1, 2, k = 1, 2, 3, 4)$ stand for the quasi-ABs corresponding to the certain pair of eigenvalues χ_k, χ_k' $(k = 1, 2, 3, 4)$ that can form the SRBs.

and $\boldsymbol{\chi}_{[2]}$ (and $\boldsymbol{\chi}'_{[2]}$) corresponding to two different spectral parameters $\lambda_{[1]}$ and $\lambda_{[2]}$ to describe this formula. These results illustrate that the MI growth rate in the linear stage can be expressed by a linear combination of group velocities. In fact, only two eigenvalues $\boldsymbol{\chi}_{[1]}$ and $\boldsymbol{\chi}_{[2]}$ were employed in Ref. [46] to interpret this relationship, and the result is an approximate description. Our previous results have shown that the higher-order effects significantly affect the MI growth rate during the linear stage. In this study, we aim to refine the existing formula to ensure its compatibility with Eqs. (1), which incorporates the higher-order terms, specifically within the nondegenerate region. To achieve this, we redefine the exact link by using four different eigenvalues, instead of utilizing approximate expansions.

First, we recall the explicit relation between MI and velocity difference for the scalar SRB in the infinite NLSE hierarchy [41], as well as that for the vector SRBs in the Manakov system [46]. For the NLSE hierarchy, the SRB solution ψ_{SRB} is constructed by employing the DT, and its spectral parameter λ is parametrized by the Jukowsky transform [8,24]. The nonlinear stage of MI is described by the scalar SRB developing from an identical initial small perturbation $\delta\psi$, which can be obtained explicitly through the procedure in Refs. [8,24]. On the other hand, in the initial stage, the MI growth rate of a small amplitude perturbation on a plane wave background has been studied by linear stability analysis, and the dispersion relation between the growth rate $\mathcal{G}_{sr}$ and the perturbation frequency Q has been found [41]. Comparing the growth rate $\mathcal{G}_{sr}$ and the velocity difference $\Delta V_{gr}(\lambda_1, \lambda_2)$, the exact link between them can be presented as follows [41]:

$$\mathcal{G}_{sr} = \Delta V_{gr}\eta_r, \tag{26}$$

with η_r being a parameter depending on the spectral parameter λ. This result is significant since it is not only an exact relation to show the MI properties but a general link that holds for the different order NLSEs [41].

Further, this formula has been successfully extended to the vector SRBs in the Manakov system. Given this scenario, the exact link is provided in the following form [46]:

$$\widehat{\mathcal{G}}_{sr} = \gamma\Delta V_g(\boldsymbol{\chi}_{[1]}, \boldsymbol{\chi}_{[2]}), \tag{27}$$

with $\gamma = \alpha/2$ being a parameter that determines the width of the breather. It is very worthwhile to notice that the vector SRBs are naturally nondegenerate solutions in the Manakov system. Consequently, the link (27) is presented in this context with two different eigenvalues $\boldsymbol{\chi}_{[1]}$ and $\boldsymbol{\chi}_{[2]}$. Remarkably, Eq. (27) is an approximation formula when ignoring the higher-order term $O(\gamma^2)$. In fact, there are four independent wave modes in nondegenerate solutions, each corresponding to a unique eigenvalue. We then speculate that the relation (27) may be further refined. Moreover, the relation should involve the higher-order coefficient ϵ in the CH equations, since they can have impacts on the MI growth rate as well as the group and phase velocities.

Next, we consider the exact relation between the MI growth rate and the linear combination of group velocities of the SRBs in the framework of the CH equations. Inspired by previous thought [41,46], the formula of MI growth rate for the vector SRBs in Eqs. (1) in the linear stage can be derived by considering $Q = \omega + i\alpha$ as the small initial perturbation frequency. In fact, for the MI described by the ABs, we usually set $Q = \omega$ as a real perturbation frequency while $Q = i\alpha$ as an imaginary frequency for the MI described by the KMS. In this way, we set $Q = \omega + i\alpha$ as a complex frequency for the general breather. Based on the aforementioned findings, the physical properties of vector SRBs are influenced by either the group velocity relationship between two quasi-ABs (reflecting the delay mechanism of growth of the small localized perturbation during the linear stage) or the phase group velocity relationship of each quasi-AB (relevant to state transitions during the nonlinear state). From the exact expressions of the vector SRBs in Eqs. (1) (see Appendix B: Higher-order breather solutions via DT), the MI growth rate is closely related to the absolute difference between two group

velocities of different quasi-ABs, as shown in Fig. 2. In fact, it is four eigenvalues, rather than two, that govern the group velocity of each quasi-AB, namely, $\boldsymbol{\chi}_{[k]}^{[1]}$, $\boldsymbol{\chi}_{[k]}^{[2]} = \boldsymbol{\chi}_{[k]}^{[1]} + \omega + i\alpha$ ($k = 1, 2, 3, 4$). Therefore, one can expect that the growth rate $\mathcal{G}$ in the linear stage is in direct proportion to the combination of two groups of group velocities $V_g(\boldsymbol{\chi}_{[k_1]}^{[1]})$ [or $V_g(\boldsymbol{\chi}_{[k_1]}^{[2]})$] and $V_g(\boldsymbol{\chi}_{[k_2]}^{[1]})$ [or $V_g(\boldsymbol{\chi}_{[k_2]}^{[2]})$]. Each of them corresponds to two eigenvalues $\boldsymbol{\chi}_{[k]}^{[1]}$, $\boldsymbol{\chi}_{[k]}^{[2]}$ and the MI growth rate $\mathcal{G}$ (19) obeys the following equation:

$$\begin{aligned}\mathcal{G} &= \varepsilon \Delta V_g\big(\boldsymbol{\chi}_{[1]}^{[1]}, \boldsymbol{\chi}_{[1]}^{[2]}, \boldsymbol{\chi}_{[2]}^{[1]}, \boldsymbol{\chi}_{[2]}^{[2]}\big) \\ &= \varepsilon\big[c_1 V_g\big(\boldsymbol{\chi}_{[1]}^{[1]}\big) + c_2 V_g\big(\boldsymbol{\chi}_{[1]}^{[2]}\big) \\ &\quad + c_3 V_g\big(\boldsymbol{\chi}_{[2]}^{[1]}\big) + c_4 V_g\big(\boldsymbol{\chi}_{[2]}^{[2]}\big)\big], \end{aligned} \tag{28}$$

with c_1–c_4 being four real parameters that accounting for the contribution degree of each $V_g(\cdot)$. Here, $\Delta V_g(\cdot_1, \cdot_2, \cdot_3, \cdot_4) = c_1 V_g(\cdot_1) + c_2 V_g(\cdot_2) + c_3 V_g(\cdot_3) + c_4 V_g(\cdot_4)$ is a function of four variables and $V_g(\cdot)$ is a function of one variable,

$$\begin{aligned} V_g(\cdot) = \epsilon \Big\{ & 6\omega\,\mathrm{Im}(\cdot)\Big[\mathrm{Re}(\cdot) + \frac{\omega}{2}\Big] + 3\alpha[\mathrm{Re}(\cdot) + \omega]^2 \\ & - \alpha[3\,\mathrm{Im}(\cdot)^2 + 3\alpha\,\mathrm{Im}(\cdot) + \alpha^2]\Big\} \\ & + \alpha\,\mathrm{Re}(\cdot) + \omega\,\mathrm{Im}(\cdot) + \omega\alpha - 2\epsilon\alpha\boldsymbol{a}^2. \end{aligned} \tag{29}$$

Equation (28) describes the exact link between the linear MI and vector SRBs in the CH equation (1). We can further delve into Eq. (28) from several perspectives. First, the right-hand side of Eq. (28) encapsulates group velocities described by four different eigenvalues. This indicates that, in a nondegenerate scenario, the evolution of the initial small localized perturbations for the first-order SRB is influenced by four eigenvalues simultaneously during the linear stage. While in the nonlinear stage, the two quasi-ABs evolved from the initial perturbation are controlled by two different sets of characteristics. Second, the parameters c_1–c_4 determine the magnitude of the contributions from these eigenvalues. In fact, we can utilize β to depict the discontinuous variation (intensity) of degeneracy. When the absolute value of $|\beta|$ is less than or equal to β_c (a critical value that distinguishes between degenerate and nondegenerate solutions), the solution represents a degenerate case (and, conversely, a nondegenerate case when it is greater). As the absolute value of β gradually approaches β_c, and $\boldsymbol{\chi}'$ approaches $-\boldsymbol{\chi}$ ($\boldsymbol{\chi} = \boldsymbol{\chi}_k$, $k = 1, 2, 3, 4$), then the degeneracy property of the solution disappears, and it finally becomes a degenerate one. We hypothesize that, during this process, the contribution of each eigenvalue and its determined group velocity to the growth rate of initial perturbations will change accordingly. Therefore, the values of four parameters c_1–c_4 should also be adjusted accordingly to reflect the varying degrees of contribution of the aforementioned eigenvalues to the growth of initial perturbations. This adjustment will enhance the matching degree between both sides of Eq. (28). Unfortunately, we have not yet discovered a precise method to determine the coefficients c_1–c_4. Finally, it is worth noting that each expression of group velocity incorporates the higher-order terms ϵ, whose changes can significantly affect the group velocity described by each eigenvalue.

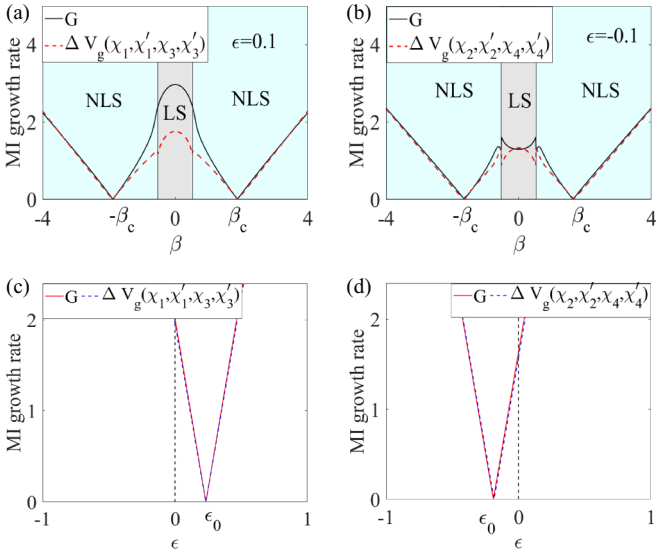

FIG. 10. (a), (b) The MI growth rate $\mathcal{G}$ and the group velocity linear combination $\varepsilon\Delta V_g(\boldsymbol{\chi}_{[1]}^{[1]}, \boldsymbol{\chi}_{[1]}^{[2]}, \boldsymbol{\chi}_{[2]}^{[1]}, \boldsymbol{\chi}_{[2]}^{[2]})$, $\boldsymbol{\chi}_{[1]}^{[1]} = \boldsymbol{\chi}_1$ (or $\boldsymbol{\chi}_2$), $\boldsymbol{\chi}_{[2]}^{[1]} = \boldsymbol{\chi}_3$ (or $\boldsymbol{\chi}_4$) with the change of β. The acronyms "LS" and "NLS" in the two panels of the first row stand for "degenerate linear stage" and "nondegenerate linear stage." Other parameters are $a = 1, \alpha = 0.2, \omega = 1.2$ and (c) $\varepsilon = 0.2$, (d) $\varepsilon = 0.17$. (c),(d) The MI growth rate $\mathcal{G}$ and the combination of group velocity $\varepsilon\Delta V_g(\boldsymbol{\chi}_{[1]}^{[1]}, \boldsymbol{\chi}_{[1]}^{[2]}, \boldsymbol{\chi}_{[2]}^{[1]}, \boldsymbol{\chi}_{[2]}^{[2]})$, $\boldsymbol{\chi}_{[1]}^{[1]} = \boldsymbol{\chi}_1$ (or $\boldsymbol{\chi}_2$), $\boldsymbol{\chi}_{[2]}^{[1]} = \boldsymbol{\chi}_3$ (or $\boldsymbol{\chi}_4$) with the change of ϵ. At a certain point $\epsilon = \epsilon_0$ of each panel in the lower row, the MI growth rate $\mathcal{G} = 0$. Other parameters are $a = 1, \alpha = 0.2, \omega = 1.2, \beta = 1$.

Consequently, any modification to this parameter has the potential to trigger changes in the group velocity difference between two quasi-ABs, subsequently influencing the growth rate $\mathcal{G}$. This observation aligns perfectly with our previous conclusions. This formula (28) represents a significant advancement from previous result [46]. Not only does it explain the relationship between the vector SRBs in the nondegenerate region and the MI growth rate, but, crucially, it accounts for the group velocity determined by four eigenvalues, rather than relying on a higher-order approximation of α. In addition, the significance of the formula also lies in its ability to facilitate a exact understanding of linear MI and nondegenerate SRBs subjected to the higher-order effects.

In order to further confirm our results, we provide several numerical examples that illustrate and reinforce our results. First, we compare the MI growth rate $\mathcal{G}$ via linear stability analysis with our new formula $\Delta V_g(\boldsymbol{\chi}_{[1]}^{[1]}, \boldsymbol{\chi}_{[1]}^{[2]}, \boldsymbol{\chi}_{[2]}^{[1]}, \boldsymbol{\chi}_{[2]}^{[2]})$ in the whole regime. When $\boldsymbol{\chi}_{[1]}^{[1]} = \boldsymbol{\chi}_1$, $\boldsymbol{\chi}_{[2]}^{[1]} = \boldsymbol{\chi}_3$ and the higher-order coefficient ϵ is set to be $\epsilon = 0.1$, the parameters are assigned as follows: $c_1 : c_2 : c_3 : c_4 \to 2 : 0 : -1 : -1$. Alternatively, when $c_1 : c_2 :, c_3 : c_4 \to 10 : -4 : -5 : -1$, the parameters are adjusted to $\boldsymbol{\chi}_{[1]}^{[1]} = \boldsymbol{\chi}_2$, $\boldsymbol{\chi}_{[2]}^{[1]} = \boldsymbol{\chi}_4$ and $\epsilon = -0.1$.

As shown in Figs. 10(a) and 10(b), one can observe that, in the nondegenerate regime, two results exhibit an agreement, whereas the formula ceases to be valid in the adjacent degenerate regime. Besides, there are two symmetric points in each panel of the first row, where the MI growth rate is zero. For simplicity, we set such two points as β_c and

$-\beta_c$ and at such two points the SRBs can be transformed into solitons. Next, we take the higher-order coefficient ϵ as the variable and compare $\mathcal{G}$ with $\Delta V_g(\boldsymbol{\chi}_{[1]}^{[1]}, \boldsymbol{\chi}_{[1]}^{[2]}, \boldsymbol{\chi}_{[2]}^{[1]}, \boldsymbol{\chi}_{[2]}^{[2]})$ in the nondegenerate regime. When $\boldsymbol{\chi}_{[1]}^{[1]} = \boldsymbol{\chi}_1$, $\boldsymbol{\chi}_{[2]}^{[1]} = \boldsymbol{\chi}_3$ and $\beta = 1$, for the first wave component, we set the parameters as $c_1 = 1, c_2 = 0, c_3 = -0.5, c_4 = -0.5$ and $c_1 = 1, c_2 = -0.4, c_3 = -0.5, c_4 = -0.1$ for the similar wave component with $\boldsymbol{\chi}_{[1]}^{[1]} = \boldsymbol{\chi}_2$, $\boldsymbol{\chi}_{[2]}^{[1]} = \boldsymbol{\chi}_4$. It is obvious that two results fit perfectly, as shown in Figs. 10(c) and 10(d). In addition, there also exists a certain point ϵ_0 in each panel of the lower row, in which the MI growth rate is zero and therefore the SRBs will be converted into other types of waves.

V. SCALAR SUPER-REGULAR BREATHERS

In this section, we will discuss the dynamic behaviours of the SRB in scalar case. We will take the Hirota equation (C1) as an example and show the amplitude profiles of the SRBs. We will further analyze the impact of higher-order effects on the solutions, as well as their influence on the relationship between the MI growth rate and their group velocities.

In fact, when $\beta_1 = \beta_2 = 0$, the fundamental solutions (3) reduce to the scalar one in the Hirota equation (C1) [39],

$$\psi_{\mathrm{SGB}[1]} = \psi_0[1 - (1 - H)\psi_{\mathrm{gb}}], \tag{30}$$

where

$$\psi_0 = a\exp(2ia^2t), \tag{31}$$

$$\psi_{\mathrm{sgb}} = 2i\boldsymbol{\chi}_i \frac{\mathcal{B}(\boldsymbol{\chi})(e^{\boldsymbol{\Gamma}} + e^{-i\boldsymbol{\Omega}}) + \mathcal{B}(\boldsymbol{\chi} + \omega + i\alpha)(e^{-\boldsymbol{\Gamma}} + e^{i\boldsymbol{\Omega}})}{\varepsilon(\boldsymbol{\chi})e^{\boldsymbol{\Gamma}} + \varepsilon(\boldsymbol{\chi} + \omega + i\alpha)e^{-\boldsymbol{\Gamma}} + \mathcal{D}e^{i\boldsymbol{\Omega}} + \mathcal{D}^* e^{-i\boldsymbol{\Omega}}}, \tag{32}$$

with

$$\mathcal{B}(\boldsymbol{\chi}) = \frac{1}{\boldsymbol{\chi}},$$
$$\varepsilon(\boldsymbol{\chi}) = 1 + \frac{2a^2}{\boldsymbol{\chi}\boldsymbol{\chi}^*},$$
$$\mathcal{D} = 1 + \frac{2a^2}{\boldsymbol{\chi}^*(\boldsymbol{\chi} + \omega + i\alpha)}. \tag{33}$$

Other parameters such as $\alpha, \omega, \epsilon, \Gamma, \Omega$ are similar to those in Eqs. (3). The available value of spectral parameter λ and eigenvalue $\boldsymbol{\chi}$ will be given in Appendix C: Particular case: The scalar SRBs. When the parameter α is sufficient small but nonzero, the breather solution (30) describes a quasi-AB. The nonlinear superposition of two different quasi ABs can generate the SRB in Eq. (C1).

Figure 11 shows the amplitude profiles of the scalar SRB. When $\epsilon = 0$, the solution (30) describes the fundamental breathers in the scalar SRB for the NLSE [8]. When $\epsilon \neq 0$, the higher-order effects will take influence on the group velocities, as shown in Fig. 11(b). When $\epsilon \neq 0$ and $V_g = V_p$, one of the quasi-ABs contained in the scalar SRB can be converted into a multipeak solitary wave [see Fig. 11(c)]. Further, Fig. 11(d) shows that when $\epsilon = \epsilon_0(\epsilon \to \infty)$, two group velocities in the SRB are equivalent to each other and the growth will be suppressed. The above results have been partially presented in Ref. [39].

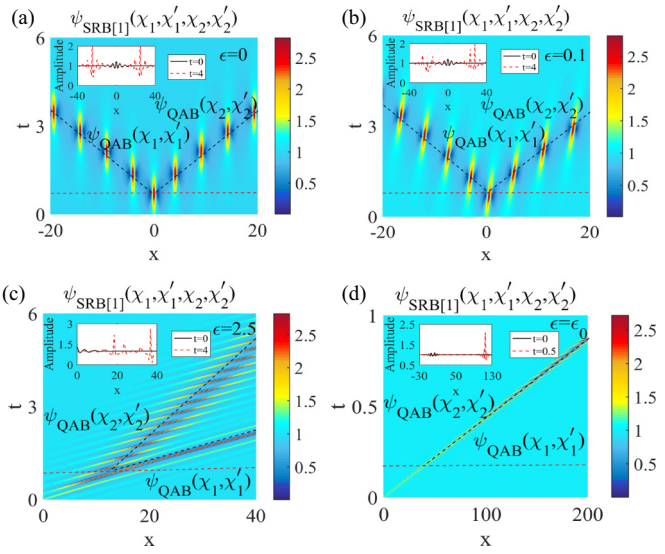

FIG. 11. The amplitude profile of the scalar SRB $\psi_{\mathrm{SRB}[1]}(\boldsymbol{\chi}_1, \boldsymbol{\chi}_2)$ in the Hirota equation with different higher-order coefficient ϵ. The parameters are $a = 1, \alpha = 0.2, \omega = 1.2, \beta = 1$.

Compared with the vector SRBs induced by the higher-order effects in Eqs. (1), the scalar SRB is merely the superposition of two quasi-ABs with opposite group velocities. However, the vector SRBs are formed by the nondegenerate quasi-ABs that are absent in the scalar system. In other words, there are two individual eigenvalues corresponding to two different wave modes in each fundamental quasi-AB for the vector SRBs. On the other hand, the fundamental quasi-AB merely consists of one spectral parameter for the scalar SRB. This distinct difference between the scalar and vector SRBs can be attribute to the additional wave components taken into account in the coupled systems. Therefore, it is meaningful for the extension of SRBs to the vector fields.

VI. NUMERICAL SIMULATION

In this section, we will employ the approximate initial conditions in simplified forms to excite the fundamental and second-order solutions for the SRBs in Eqs. (1). Moreover, we also excite the converted SRBs by the numerical simulation, using both the exact initial condition and an approximate one.

The above vector SRBs can be excited by numerical simulation, utilizing the exact initial condition [see Eqs. (B4) in Appendix B: Higher-order breather solutions via DT]. Additionally, we present an alternative way to excite them by using the initial conditions in the form of periodic perturbation of the vector plane wave localized in x, which shows similarities to that employed in the Manakov system:

$$\psi^{(j)} = \psi_0^{(j)}[1 + \varepsilon L_p(x/x_W)\cos(\omega x)], \tag{34}$$

where $\psi_0^{(j)}$ are the vector background plane waves as those in Eqs. (3), and the localized function $L_p(x/x_W)$ is represented either by the sech function $L_p(x/x_W) = \mathrm{sech}(x/x_W)$ or by a Gaussian function $L_p(x/x_W) = \exp(-x^2/x_W^2)$ with x_W being the width of the localization, which is comparable to that of the exact solutions, namely $1/\alpha$.

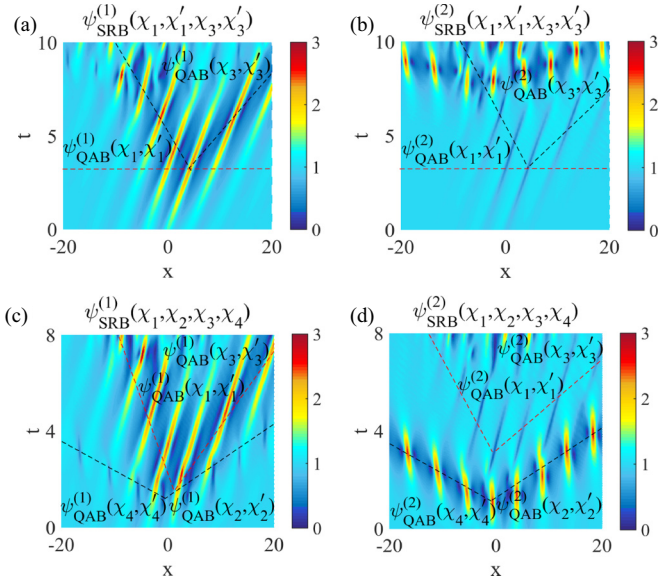

FIG. 12. Amplitude profiles of (a), (b) the fundamental SRBs and (c), (d) the second-order SRBs by the numerical simulation started with Eq. (34). Dashed lines in each panel illustrate the group velocities of individual breathers. The parameters are $a = 1, \alpha = 0.2, \omega = 1.2, \beta = 1, \epsilon = 0.1$.

Figure 12 shows the amplitude evolution of fundamental SRBs $|\psi^{(j)}_{\mathrm{SRB}[1]}(\chi_1, \chi_1', \chi_3, \chi_3')|$ and the second-order SRBs $|\psi^{(j)}_{\mathrm{SRB}[2]}(\chi_1, \chi_1', \chi_2, \chi_2', \chi_3, \chi_3', \chi_4, \chi_4')|$ obtained from the numerical simulations developed from the *approximate initial condition* (34). The plane waves are unstable and develop into two quasi-ABs with opposite group velocities. Figure 13 shows the amplitude evolution of fundamental and second-order SRBs excited by the *exact initial conditions*. Such profiles are nearly identical to those in Figs. 1 and 2. On the other hand, Fig. 14 shows the amplitude evolutions of the converted SRBs described by $|\psi^{(j)}_{\mathrm{SRB}[1]}(\chi_1, \chi_1', \chi_2, \chi_2', \chi_3, \chi_3', \chi_4, \chi_4')|$, which are excited by the exact initial condition and approximate initial condition. Although the amplitude profiles of their initial conditions are different (unfortunately, we are unable to find an approximate representation for numerical excitation similar to that for the analytical initial case), similar wave patterns are observed to be excited. In contrast to the general SRBs, the converted waves evolve along a certain direction and exhibit the solitary-wave state with several peaks. Comparing the two panels in the figure, it is obvious that they exhibit similar amplitude profiles in the initial stage while the right panel shows unstable structures after a short time.

VII. CONCLUSION

In conclusion, we have presented the solutions of the vector SRBs within the framework of the CH equations incorporating the higher-order effects. These vector SRBs, which arise from the nonlinear superposition of two individual nondegenerate quasi-ABs linked to two different eigenvalues, represent a significant advancement compared to those in the scalar models. Our investigation delved deeper into the influence of higher-order effects on the vector SRBs, shedding light on

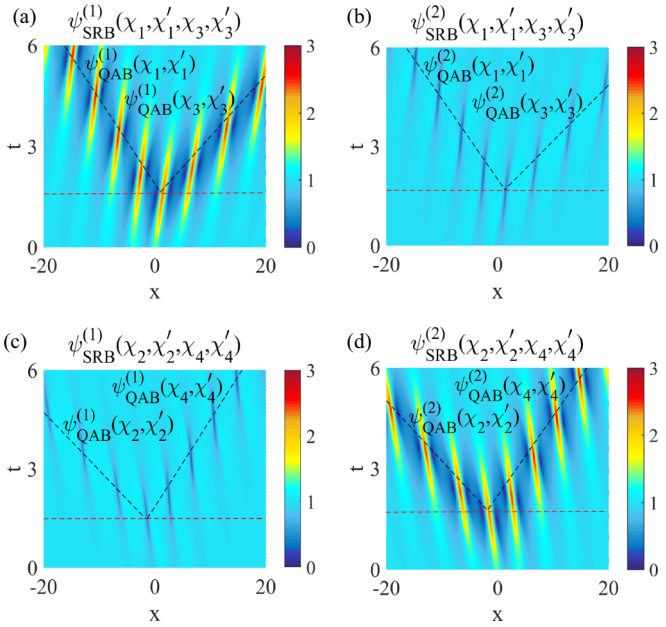

FIG. 13. Amplitude profiles of the fundamental SRBs involving two quasi-ABs corresponding to two different eigenvalues (a), (b) χ_1, χ_1' and χ_3, χ_3' and (c), (d) χ_2, χ_2' and χ_4, χ_4' developed from the exact initial conditions by the numerical simulation. Red dashed lines in each panel serve to delineate the linear and nonlinear stage of evolution. The dark dashes illustrate the group velocities of two individual fundamental breathers. The parameters are $a = 1, \alpha = 0.2, \omega = 1.2, \beta = 1, \epsilon = 0.1$.

their impact during both the linear and nonlinear stages of MI. Higher-order effects can increase the growth time of the linear stage and reshape the evolution modes of the nonlinear stage. In particular, a significant finding is that the presence of the higher-order term can neutralize the absolute difference in

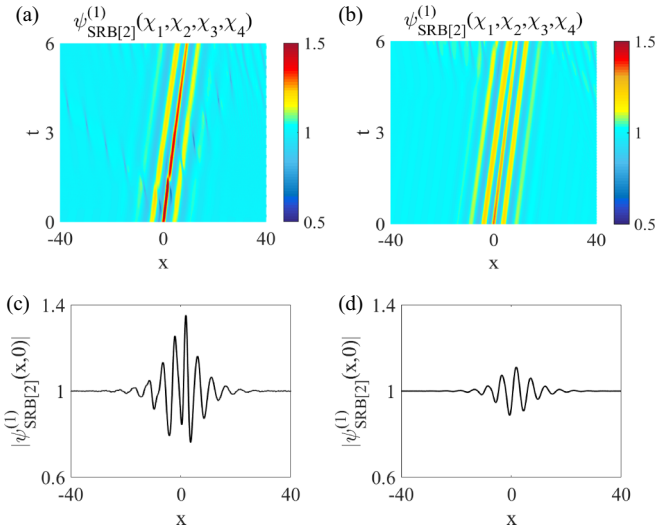

FIG. 14. Amplitude profiles of the converted SRBs excited by the (a) exact initial condition and (b) approximate initial condition through the numerical simulations, respectively. The cross sections of the (c) exact initial conditions and (d) approximate conditions. The parameters are $a = 1, \alpha = 0.2, \omega = 1.2, \beta = \beta_c, \epsilon = 0.1$.

group velocities inherent in SRBs. This phenomenon cannot be observed in the Manakov system nor in a series of scalar models such as the NLSE and the complex modified KdV equation. Further analysis on the MI has unveiled the intricate relationship between the vector SRBs and MI growth rate under the influence of higher-order effects. We have refined the existing formulas, eliminating the necessity to neglect higher-order terms from the Taylor expansion of α. Instead, we have utilized four distinct eigenvalues for a more comprehensive description. In the nondegenerate regime, our formula exhibits a good fit. We have also reduced the results to the case of scalar SRBs. We have finally excited both the SRBs as well as their converted modes by the numerical simulation started with the localized periodic initial condition. Our study not only advances the theoretical understanding of vector SRBs with higher-order effects, but also paves the way for practical applications and the interpretation of related experimental phenomena.

No new data were created or analyzed in this study.

ACKNOWLEDGMENTS

We express our sincere thanks to the referees and to all the members of our discussion group for their valuable comments. This work is supported by the National Natural Science Foundation of China Grant No. 12375002.

Author contributions are as follows: L.P.: analytical calculations, analysis, numerical simulation, and writing; L.W.: idea of this paper, analytical calculations, analysis, physics, numerical simulation, writing, and supervision; L.L.: numerical simulation.

APPENDIX A: VECTOR BREATHER SOLUTIONS VIA DT

The fundamental solutions for the quasi ABs as well as the vector SRBs for Eqs. (1) can be derived via the DT [56]. Here we present more details. Equations (1) admit the following Lax pair:

$$\boldsymbol{\Psi}_x = \boldsymbol{U}\boldsymbol{\Psi}, \quad \boldsymbol{\Psi}_t = \boldsymbol{V}\boldsymbol{\Psi}, \tag{A1}$$

where $\boldsymbol{\Psi} = (R, S, W)^T$ (T denotes a matrix transpose) and

$$\boldsymbol{U} = i\begin{pmatrix} \lambda & \psi^{(1)*} & \psi^{(2)*} \\ \psi^{(1)} & 0 & 0 \\ \psi^{(2)} & 0 & 0 \end{pmatrix}, \tag{A2}$$

$$\boldsymbol{V} = \lambda^3 V_3 + \lambda^2 V_2 + \lambda V_1 + V_0, \tag{A3}$$

with

$$\begin{aligned} V_3 &= \frac{i}{2}(I+\Lambda), V_2 = \frac{i}{4}(I+\Lambda) + i\epsilon Q, \\ V_1 &= \frac{i}{2}Q + \epsilon\Lambda(Q_x - iQ^2) + i\epsilon\Lambda_0 \boldsymbol{a}^2, \\ V_0 &= \frac{1}{2}\Lambda(Q_x - iQ^2) + \frac{\epsilon}{4}(I-\Lambda)(Q^2 - 2\boldsymbol{a}^2)_x - 3i\epsilon Q\boldsymbol{a}^2, \end{aligned} \tag{A4}$$

and

$$\Lambda = \begin{pmatrix} 1 & 0 & 0 \\ 0 & -1 & 0 \\ 0 & 0 & -1 \end{pmatrix}, \quad \Lambda_0 = \begin{pmatrix} 1 & 0 & 0 \\ 0 & -2 & 0 \\ 0 & 0 & -2 \end{pmatrix}, \tag{A5}$$

$$Q = \begin{pmatrix} 0 & \psi^{(1)*} & \psi(2)* \\ \psi^{(1)} & 0 & 0 \\ \psi^{(2)} & 0 & 0 \end{pmatrix}. \tag{A6}$$

In the above equations, the asterisk "$*$" represents the complex conjugation, $\boldsymbol{a}^2 = |\psi^{(1)}|^2 + |\psi^{(2)}|^2$, and λ is the spectral parameter which satisfies the following relation with the eigenvalue $\boldsymbol{\chi}$,

$$\lambda = \boldsymbol{\chi} - \frac{a_1^2}{\boldsymbol{\chi} + \beta_1} - \frac{a_2^2}{\boldsymbol{\chi} + \beta_2}. \tag{A7}$$

The compatibility condition $\boldsymbol{U} - \boldsymbol{V} + [\boldsymbol{U}, \boldsymbol{V}] = 0$ gives rise to the CH equations (1). Taking the seed solutions as the vector background plane waves,

$$\begin{aligned} \psi_0^{(j)} = a_j \exp\Big\{ i\beta_j x + i\Big[a_1^2 + a_2^2 - \frac{\beta_j^2}{2} + \epsilon\big(\beta_j^3 - 3\big(a_1^2 + a_2^2\big) \\ \times \beta_j - 3a_j^2(\beta_1 + \beta_2)\big)\Big] t\Big\}, \quad j = 1, 2, \end{aligned}$$

one can obtain the eigenfunctions of the linear system (A1) as

$$\begin{aligned} R_{[k]}^{[0]} &= c_1\varphi_{[k]}^{[1]} + c_2\varphi_{[k]}^{[2]} + c_3\varphi_{[k]}^{[3]}, \\ S_{[k]}^{[0]} &= \psi_0^{(1)}\left(c_1\frac{\varphi_{[k]}^{[1]}}{\boldsymbol{\chi}_{[k]}^{[1]} + \beta_1} + c_2\frac{\varphi_{[k]}^{[2]}}{\boldsymbol{\chi}_{[k]}^{[2]} + \beta_1} + c_3\frac{\varphi_{[k]}^{[3]}}{\boldsymbol{\chi}_{[k]}^{[3]} + \beta_1} \right), \\ W_{[k]}^{[0]} &= \psi_0^{(2)}\left(c_1\frac{\varphi_{[k]}^{[1]}}{\boldsymbol{\chi}_{[k]}^{[1]} + \beta_2} + c_2\frac{\varphi_{[k]}^{[2]}}{\boldsymbol{\chi}_{[k]}^{[2]} + \beta_2} + c_3\frac{\varphi_{[k]}^{[3]}}{\boldsymbol{\chi}_{[k]}^{[3]} + \beta_2} \right), \end{aligned} \tag{A8}$$

where

$$\begin{aligned} \varphi_{[k]}^{[l]} &= \exp\left[i\boldsymbol{\chi}_{[k]}^{[l]} x + i\left(\epsilon\boldsymbol{\chi}_{[k]}^{[l]3} + \frac{\boldsymbol{\chi}_{[k]}^{[l]2}}{2} - 2\epsilon\boldsymbol{a}^2\boldsymbol{\chi}_{[k]}^{[l]} - \epsilon\boldsymbol{a}^2 \right) t \right], \\ & l = 1, 2, 3, \end{aligned} \tag{A9}$$

with $k = 1, 2, \ldots, N$ denoting the order of the obtained breather solutions. Moreover, the parameters c_l ($l = 1, 2, 3$) are three arbitrary real constants, and $\boldsymbol{\chi}_{[k]}^{[1]}$ is the eigenvalue obtained form Eq. (11), and denoted as

$$\begin{aligned} \boldsymbol{\chi}_{[k]}^{[2]} &= \boldsymbol{\chi}_{[k]}^{[1]} + \omega + i\alpha, \\ \boldsymbol{\chi}_{[k]}^{[3]} &= -\boldsymbol{\chi}_{[k]}^{[1]} - \frac{a_1^2}{\boldsymbol{\chi}_{[k]}^{[1]} + \beta_1} - \frac{a_2^2}{\boldsymbol{\chi}_{[k]}^{[1]} + \beta_2} - \omega - i\alpha. \end{aligned}$$

For simplicity, we take $c_1 = c_2 = 1, c_3 = 0$. Then the fundamental breather solutions read as

$$\begin{aligned} \psi_1^{(1)} &= \psi_0^{(1)} + (\lambda_{[k]}^* - \lambda_{[k]})\frac{R_{[k]}^{[0]*} S_{[k]}^{[0]}}{\big|R_{[k]}^{[0]}\big|^2 + \big|S_{[k]}^{[0]}\big|^2 + \big|W_{[k]}^{[0]}\big|^2}, \\ \psi_1^{(2)} &= \psi_0^{(1)} + (\lambda_{[k]}^* - \lambda_{[k]})\frac{R_{[k]}^{[0]*} W_{[k]}^{[0]}}{\big|R_{[k]}^{[0]}\big|^2 + \big|S_{[k]}^{[0]}\big|^2 + \big|W_{[k]}^{[0]}\big|^2}, \end{aligned} \tag{A10}$$

which can be also written as the form of Eqs. (3).

APPENDIX B: HIGHER-ORDER BREATHER SOLUTIONS VIA DT

We perform the iteration of DT to obtain the exact solutions for the fundamental SRBs,

$$\begin{aligned}\psi^{(1)}_{\mathrm{SRB}[1]} &= \psi^{(1)}_2 = \psi^{(1)}_1 + (\lambda^*_{[2]} - \lambda_{[2]}) \\ &\quad \times \frac{R^{[1]*}_{[2]} S^{[1]}_{[2]}}{\left|R^{[1]}_{[2]}\right|^2 + \left|S^{[1]}_{[2]}\right|^2 + \left|W^{[1]}_{[2]}\right|^2}, \\ \psi^{(2)}_{\mathrm{SRB}[1]} &= \psi^{(2)}_2 = \psi^{(1)}_1 + (\lambda^*_{[2]} - \lambda_{[2]}) \\ &\quad \times \frac{R^{[1]*}_{[2]} W^{[1]}_{[2]}}{\left|R^{[1]}_{[2]}\right|^2 + \left|S^{[1]}_{[2]}\right|^2 + \left|W^{[1]}_{[2]}\right|^2},\end{aligned} \tag{B1}$$

where

$$\begin{aligned}R^{[1]}_{[2]} &= T[1]T[0]R^{[0]}_{[2]}, \\ S^{[1]}_{[2]} &= T[1]T[0]S^{[0]}_{[2]}, \\ W^{[1]}_{[2]} &= T[1]T[0]W^{[0]}_{[2]},\end{aligned} \tag{B2}$$

with

$$\begin{aligned}T[0] &= I, \\ T[1] &= I + \frac{\lambda^*_{[1]} - \lambda_{[1]}}{\lambda_{[2]} - \lambda^*_{[1]}} \frac{\boldsymbol{\Psi}^{[0]}_{[1]} \boldsymbol{\Psi}^{[0]\dagger}_{[1]}}{\boldsymbol{\Psi}^{[0]\dagger}_{[1]} \boldsymbol{\Psi}^{[0]}_{[1]}}.\end{aligned} \tag{B3}$$

Such expressions can also be written in the following form:

$$\psi^{(j)}_{\mathrm{SRB}[2]} = \psi^{(j)}_0 \frac{e^{X_1} H^{(j)}_1 + e^{X_2} H^{(j)}_2 + 2e^{X_3}\left(M^{(j)}_1 e^{iY_1} H^{(j)}_{31} + M^{(j)}_2 e^{-iY_1} H^{(j)}_{32} + e^{iY_2} H^{(j)}_{33} + e^{-iY_2} H^{(j)}_{34}\right)}{e^{X_1} H_1 + e^{X_2} H_2 + 2e^{X_3}(M_1 e^{iY_1} H_{31} + M_2 e^{-iY_1} H_{32} + e^{iY_2} H_{33} + e^{-iY_2} H_{34})}, \tag{B4}$$

where

$$\begin{aligned}H_1 &= A_1 + A_2[\cosh(\boldsymbol{\Gamma}_1 - \gamma_1) + \cos(\boldsymbol{\Omega}_1 + \delta_1)], \\ H_2 &= B_1 + B_2[\cosh(\boldsymbol{\Gamma}_2 - \gamma_2) + \cos(\boldsymbol{\Omega}_2 + \delta_2)], \\ H_{31} &= \cosh(\boldsymbol{\Gamma}_{31} + \gamma_{31}) + \cosh(\boldsymbol{\Gamma}_{32} + \gamma_{32}) \\ &\quad + \cos(\boldsymbol{\Omega}_{31} + \delta_{31}) + \cos(\boldsymbol{\Omega}_{32} + \delta_{32}), \\ H_{32} &= \cosh(\boldsymbol{\Gamma}_{31} - \gamma_{31}) + \cosh(\boldsymbol{\Gamma}_{32} - \gamma_{32}) \\ &\quad + \cos(\boldsymbol{\Omega}_{31} - \delta_{31}) + \cos(\boldsymbol{\Omega}_{32} - \delta_{32}), \\ H_{33} &= N_1 \cosh(\boldsymbol{\Gamma}_{31} + \gamma_{33}) + N_2 \cosh(\boldsymbol{\Gamma}_{32} + \gamma_{34}) \\ &\quad + N_1 \cos(\boldsymbol{\Omega}_{31} + \delta_{33}) + N_2 \cos(\boldsymbol{\Omega}_{32} + \delta_{34}), \\ H_{34} &= N_1 \cosh(\boldsymbol{\Gamma}_{31} - \gamma_{33}) + N_2 \cosh(\boldsymbol{\Gamma}_{32} - \gamma_{34}) \\ &\quad + N_1 \cos(\boldsymbol{\Omega}_{31} - \delta_{33}) + N_2 \cos(\boldsymbol{\Omega}_{32} - \delta_{34}), \\ M_1 &= \sqrt{a_1 a_2 c_3 c_4}, \quad M_2 = \sqrt{a_3 a_4 c_1 c_2},\end{aligned} \tag{B5}$$

and

$$\begin{aligned}H^{(j)}_1 &= A^{(j)}_1 + A^{(j)}_2\left[\cosh\left(\boldsymbol{\Gamma}_1 - \gamma^{(j)}_1\right) + \cos\left(\boldsymbol{\Omega}_1 + \delta^{(j)}_1\right)\right], \\ H^{(j)}_2 &= B^{(j)}_1 + B^{(j)}_2\left[\cosh\left(\boldsymbol{\Gamma}_2 - \gamma^{(j)}_2\right) + \cos\left(\boldsymbol{\Omega}_2 + \delta^{(j)}_2\right)\right], \\ H^{(j)}_{31} &= \cosh\left(\boldsymbol{\Gamma}_{31} + \gamma^{(j)}_{31}\right) + \cosh\left(\boldsymbol{\Gamma}_{32} + \gamma^{(j)}_{32}\right) \\ &\quad + \cos\left(\boldsymbol{\Omega}_{31} + \delta^{(j)}_{31}\right) + \cos\left(\boldsymbol{\Omega}_{32} + \delta^{(j)}_{32}\right) \\ H^{(j)}_{32} &= \cosh\left(\boldsymbol{\Gamma}_{31} - \gamma^{(j)}_{31}\right) + \cosh\left(\boldsymbol{\Gamma}_{32} - \gamma^{(j)}_{32}\right) \\ &\quad + \cos\left(\boldsymbol{\Omega}_{31} - \delta^{(j)}_{31}\right) + \cos\left(\boldsymbol{\Omega}_{32} - \delta^{(j)}_{32}\right) \\ H^{(j)}_{33} &= N^{(j)}_1 \cosh\left(\boldsymbol{\Gamma}_{31} + \gamma^{(j)}_{33}\right) + N^{(j)}_2 \cosh\left(\boldsymbol{\Gamma}_{32} + \gamma^{(j)}_{34}\right) \\ &\quad + N^{(j)}_1 \cos\left(\boldsymbol{\Omega}_{31} + \delta^{(j)}_{33}\right) + N^{(j)}_2 \cos\left(\boldsymbol{\Omega}_{32} + \delta^{(j)}_{34}\right) \\ H^{(j)}_{34} &= N^{(j)}_1 \cosh\left(\boldsymbol{\Gamma}_{31} - \gamma^{(j)}_{33}\right) + N^{(j)}_2 \cosh\left(\boldsymbol{\Gamma}_{32} - \gamma^{(j)}_{34}\right) \\ &\quad + N^{(j)}_1 \cos\left(\boldsymbol{\Omega}_{31} - \delta^{(j)}_{33}\right) + N^{(j)}_2 \cos\left(\boldsymbol{\Omega}_{32} - \delta^{(j)}_{34}\right) \\ M^{(j)}_1 &= \sqrt{a^{(j)}_1 a^{(j)}_2 c^{(j)}_3 c^{(j)}_4}, \quad M^{(j)}_2 = \sqrt{a^{(j)}_3 a^{(j)}_4 c^{(j)}_1 c^{(j)}_2},\end{aligned} \tag{B6}$$

with

$$\begin{aligned}X_1 &= -2\boldsymbol{\chi}^{[1]}_{[1]i} x + 2\big[\epsilon\left(\boldsymbol{\chi}^{[1]3}_{[1]i} - 3\boldsymbol{\chi}^{[1]}_{[1]i}\boldsymbol{\chi}^{[1]2}_{[1]r}\right) \\ &\quad + \boldsymbol{\chi}^{[1]}_{[1]i}\boldsymbol{\chi}^{[1]}_{[1]r} - 4\epsilon a^2 \boldsymbol{\chi}^{[1]}_{[1]i}\big]t, \\ X_2 &= -2\boldsymbol{\chi}^{[1]}_{[2]i} x + 2\big[\epsilon\left(\boldsymbol{\chi}^{[1]3}_{[2]i} - 3\boldsymbol{\chi}^{[1]}_{[2]i}\boldsymbol{\chi}^{[1]2}_{[2]r}\right) \\ &\quad + \boldsymbol{\chi}^{[1]}_{[2]i}\boldsymbol{\chi}^{[1]}_{[2]r} - 4\epsilon a^2 \boldsymbol{\chi}^{[1]}_{[2]i}\big]t, \\ X_3 &= -\left(\boldsymbol{\chi}^{[1]}_{[1]i} + \boldsymbol{\chi}^{[1]}_{[2]i}\right)x + \big[\epsilon\left(\boldsymbol{\chi}^{[1]3}_{[1]i} - \boldsymbol{\chi}^{[1]3}_{[2]i} + 3\boldsymbol{\chi}^{[1]}_{[1]i}\boldsymbol{\chi}^{[1]2}_{[2]r}\right. \\ &\quad \left. - 3\boldsymbol{\chi}^{[1]}_{[1]i}\boldsymbol{\chi}^{[1]2}_{[1]r}\right) + \left(\boldsymbol{\chi}^{[1]}_{[1]i}\boldsymbol{\chi}^{[1]}_{[2]r} - \boldsymbol{\chi}^{[1]}_{[1]i}\boldsymbol{\chi}^{[1]}_{[2]r}\right) \\ &\quad + 4\epsilon a^2\left(\boldsymbol{\chi}^{[1]}_{[2]i} - \boldsymbol{\chi}^{[1]}_{[1]i}\right)\big]t + \boldsymbol{\Gamma}_{31}, \\ Y_1 &= \left(\boldsymbol{\chi}^{[1]}_{[1]r} - \boldsymbol{\chi}^{[1]}_{[2]r}\right)x + \big[\epsilon\left(\boldsymbol{\chi}^{[1]3}_{[1]r} - \boldsymbol{\chi}^{[1]3}_{[2]r} + 3\boldsymbol{\chi}^{[1]}_{[2]r}\boldsymbol{\chi}^{[1]2}_{[2]i}\right. \\ &\quad \left. - 3\boldsymbol{\chi}^{[1]}_{[1]r}\boldsymbol{\chi}^{[1]2}_{[1]i}\right) + \tfrac{1}{2}\left(\boldsymbol{\chi}^{[1]2}_{[1]r} - \boldsymbol{\chi}^{[1]2}_{[2]r} + \boldsymbol{\chi}^{[1]2}_{[2]i} - \boldsymbol{\chi}^{[1]2}_{[1]i}\right) \\ &\quad - 4\epsilon a^2\left(\boldsymbol{\chi}^{[1]}_{[1]r} - \boldsymbol{\chi}^{[1]}_{[2]r}\right)\big]t + \boldsymbol{\Omega}_{32}, \\ Y_2 &= \left(\boldsymbol{\chi}^{[1]}_{[1]r} + \boldsymbol{\chi}^{[1]}_{[2]r}\right)x + \big[\epsilon\left(\boldsymbol{\chi}^{[1]3}_{[1]r} + \boldsymbol{\chi}^{[1]3}_{[2]r} - 3\boldsymbol{\chi}^{[1]}_{[2]r}\boldsymbol{\chi}^{[1]2}_{[2]i}\right. \\ &\quad \left. - 3\boldsymbol{\chi}^{[1]}_{[1]r}\boldsymbol{\chi}^{[1]2}_{[1]i}\right) + \tfrac{1}{2}\left(\boldsymbol{\chi}^{[1]2}_{[1]r} + \boldsymbol{\chi}^{[1]2}_{[2]r} - \boldsymbol{\chi}^{[1]2}_{[2]i} - \boldsymbol{\chi}^{[1]2}_{[1]i}\right) \\ &\quad - 4\epsilon a^2\left(\boldsymbol{\chi}^{[1]}_{[1]r} + \boldsymbol{\chi}^{[1]}_{[2]r}\right)\big]t + \boldsymbol{\Omega}_{32}, \\ N_1 &= \sqrt{(a_1 c_3 + |b_1|^2)(a_2 c_4 + |b_2|^2)}, \\ N_2 &= \sqrt{(a_1 c_4 + b_1 b^*_2)(a_2 c_3 + b^*_1 b_2)}, \\ N^{(j)}_1 &= \sqrt{\left(a^{(j)}_1 c^{(j)}_3 + \left|b^{(j)}_1\right|^2\right)\left(a^{(j)}_2 c^{(j)}_4 + \left|b^{(j)}_2\right|^2\right)}, \\ N^{(j)}_2 &= \sqrt{\left(a^{(j)}_1 c^{(j)}_4 + b^{(j)}_1 b^{(j)*}_2\right)\left(a^{(j)}_2 c^{(j)}_3 + b^{(j)*}_1 b^{(j)}_2\right)},\end{aligned} \tag{B7}$$

and

$$\begin{aligned}A_1 &= |b_1|^2 + |b_2|^2, \quad A_2 = 2|b_1||b_2|, \\ B_1 &= |b_3|^2 + |b_4|^2, \quad B_2 = 2|b_3||b_4|, \\ A^{(j)}_1 &= \left|b^{(j)}_1\right|^2 + \left|b^{(j)}_2\right|^2, \quad A^{(j)}_2 = 2\left|b^{(j)}_1\right|\left|b^{(j)}_2\right|, \\ B^{(j)}_1 &= \left|b^{(j)}_3\right|^2 + \left|b^{(j)}_4\right|^2, \quad B^{(j)}_2 = 2\left|b^{(j)}_3\right|\left|b^{(j)}_4\right|,\end{aligned} \tag{B8}$$

$$
\begin{aligned}
&\mathbf{\Gamma}_1 = \alpha x + V_g\big(\chi_{[1]}^{[1]}\big)t, \quad \gamma_1 = \frac{1}{2}\ln\frac{b_1 b_2^*}{b_1^* b_2},\\
&\gamma_1^{(j)} = \frac{1}{2}\ln\frac{b_1^{(j)} b_2^{(j)*}}{b_1^{(j)*} b_2^{(j)}},\\
&\mathbf{\Gamma}_2 = \alpha x + V_g\big(\chi_{[2]}^{[1]}\big)t, \quad \gamma_2 = \frac{1}{2}\ln\frac{b_3 b_4^*}{b_3^* b_4},\\
&\gamma_2^{(j)} = \frac{1}{2}\ln\frac{b_3^{(j)} b_4^{(j)*}}{b_3^{(j)*} b_4^{(j)}},\\
&\mathbf{\Gamma}_{31} = \frac{1}{2}(\mathbf{\Gamma}_1 - \mathbf{\Gamma}_2), \quad \mathbf{\Gamma}_{32} = -\alpha x + \mathbf{\Gamma}_{31},\\
&\gamma_{31} = \frac{1}{2}\ln\frac{a_1 c_3}{a_2 c_4}, \quad \gamma_{32} = \frac{1}{2}\ln\frac{a_1 c_4}{a_2 c_3},\\
&\gamma_{33} = \frac{1}{2}\ln\frac{a_1 c_3 + |b_1|^2}{a_2 c_4 + |b_2|^2}, \quad \gamma_{34} = \frac{1}{2}\ln\frac{a_1 c_4 + b_1 b_2^*}{a_2 c_3 + b_1^* b_2},\\
&\gamma_{31}^{(j)} = \frac{1}{2}\ln\frac{a_1^{(j)} c_3^{(j)}}{a_2^{(j)} c_4^{(j)}}, \quad \gamma_{32}^{(j)} = \frac{1}{2}\ln\frac{a_1^{(j)} c_4^{(j)}}{a_2^{(j)} c_3^{(j)}},\\
&\gamma_{33}^{(j)} = \frac{1}{2}\ln\frac{a_1^{(j)} c_3^{(j)} + \big|b_1^{(j)}\big|^2}{a_2^{(j)} c_4^{(j)} + \big|b_2^{(j)}\big|^2},\\
&\gamma_{34}^{(j)} = \frac{1}{2}\ln\frac{a_1^{(j)} c_4^{(j)} + b_1^{(j)} b_2^{(j)*}}{a_2^{(j)} c_3^{(j)} + b_1^{(j)*} b_2^{(j)}},\\
&\mathbf{\Omega}_1 = \omega x + V_p\big(\chi_{[1]}^{[1]}\big)t, \quad \delta_1 = \arg\frac{b_1 b_2^*}{b_1^* b_2},\\
&\delta_1^{(j)} = \arg\frac{b_1^{(j)} b_2^{(j)*}}{b_1^{(j)*} b_2^{(j)}},\\
&\mathbf{\Omega}_2 = \omega x + V_p\big(\chi_{[2]}^{[1]}\big)t, \quad \delta_2 = \arg\frac{b_3 b_4^*}{b_3^* b_4},\\
&\delta_2^{(j)} = \arg\frac{b_3^{(j)} b_4^{(j)*}}{b_3^{(j)*} b_4^{(j)}},\\
&\mathbf{\Omega}_{31} = \frac{1}{2}(\mathbf{\Omega}_1 + \mathbf{\Omega}_2), \quad \mathbf{\Omega}_{32} = -\omega x + \mathbf{\Omega}_{31},\\
&\delta_{31} = \arg\frac{a_2 c_4}{a_1 c_3}, \quad \delta_{31} = \arg\frac{a_1 c_3}{a_2 c_4},\\
&\delta_{33} = \arg\frac{a_1 c_3 + |b_1|^2}{a_2 c_4 + |b_2|^2}, \quad \delta_{34} = \arg\frac{a_1 c_4 + b_1 b_2^*}{a_2 c_3 + b_1^* b_2}\\
&\delta_{31}^{(j)} = \arg\frac{a_2^{(j)} c_4^{(j)}}{a_1^{(j)} c_3^{(j)}}, \quad \delta_{31}^{(j)} = \arg\frac{a_1^{(j)} c_3^{(j)}}{a_2^{(j)} c_4^{(j)}},\\
&\delta_{33}^{(j)} = \arg\frac{a_1^{(j)} c_1^{(j)} + \big|b_1^{(j)}\big|^2}{a_2^{(j)} c_2^{(j)} + \big|b_2^{(j)}\big|^2}, \quad \delta_{34}^{(j)} = \arg\frac{a_1^{(j)} c_2^{(j)} + b_1^{(j)} b_2^{(j)*}}{a_2^{(j)} c_1^{(j)} + b_1^{(j)*} b_2^{(j)}}.
\end{aligned}
\tag{B9}
$$

Other parameters are given by

$$
\begin{aligned}
a_1 &= \frac{1}{\chi_{[1]}^{[1]*} - \chi_{[1]}^{[1]}} + \frac{1}{\chi_{[1]}^{[2]*} - \chi_{[1]}^{[1]}},\\
a_2 &= \frac{1}{\chi_{[1]}^{[2]*} - \chi_{[1]}^{[2]}} + \frac{1}{\chi_{[1]}^{[1]*} - \chi_{[1]}^{[2]}},\\
a_3 &= \frac{1}{\chi_{[1]}^{[1]*} - \chi_{[1]}^{[1]}} + \frac{1}{\chi_{[1]}^{[2]*} - \chi_{[1]}^{[1]}},\\
a_4 &= \frac{1}{\chi_{[1]}^{[2]*} - \chi_{[1]}^{[1]}} + \frac{1}{\chi_{[1]}^{[2]*} - \chi_{[1]}^{[2]}},
\end{aligned}
\tag{B10}
$$

$$
\begin{aligned}
b_1 &= \frac{1}{\chi_{[2]}^{[1]*} - \chi_{[1]}^{[1]}} + \frac{1}{\chi_{[2]}^{[2]*} - \chi_{[1]}^{[1]}},\\
b_2 &= \frac{1}{\chi_{[2]}^{[2]*} - \chi_{[1]}^{[2]}} + \frac{1}{\chi_{[2]}^{[1]*} - \chi_{[1]}^{[2]}},\\
b_3 &= \frac{1}{\chi_{[2]}^{[1]*} - \chi_{[1]}^{[1]}} + \frac{1}{\chi_{[2]}^{[2]*} - \chi_{[1]}^{[1]}},\\
b_4 &= \frac{1}{\chi_{[2]}^{[2]*} - \chi_{[1]}^{[1]}} + \frac{1}{\chi_{[2]}^{[2]*} - \chi_{[1]}^{[2]}},
\end{aligned}
\tag{B11}
$$

$$
\begin{aligned}
c_1 &= \frac{1}{\chi_{[2]}^{[1]*} - \chi_{[2]}^{[1]}} + \frac{1}{\chi_{[2]}^{[2]*} - \chi_{[2]}^{[1]}},\\
c_2 &= \frac{1}{\chi_{[2]}^{[2]*} - \chi_{[2]}^{[2]}} + \frac{1}{\chi_{[2]}^{[1]*} - \chi_{[2]}^{[2]}},\\
c_3 &= \frac{1}{\chi_{[2]}^{[1]*} - \chi_{[1]}^{[1]}} + \frac{1}{\chi_{[2]}^{[2]*} - \chi_{[1]}^{[1]}},\\
c_4 &= \frac{1}{\chi_{[2]}^{[2]*} - \chi_{[1]}^{[1]}} + \frac{1}{\chi_{[2]}^{[2]*} - \chi_{[2]}^{[2]}},
\end{aligned}
\tag{B12}
$$

and

$$
\begin{aligned}
a_1^{(j)} &= \frac{\chi_{[1]}^{[1]*} + \beta_j}{\chi_{[1]}^{[1]} + \beta_j}\frac{1}{\chi_{[1]}^{[1]*} - \chi_{[1]}^{[1]}} + \frac{\chi_{[1]}^{[2]*} + \beta_j}{\chi_{[1]}^{[1]} + \beta_j}\frac{1}{\chi_{[1]}^{[2]*} - \chi_{[1]}^{[1]}},\\
a_2^{(j)} &= \frac{\chi_{[1]}^{[2]*} + \beta_j}{\chi_{[1]}^{[2]} + \beta_j}\frac{1}{\chi_{[1]}^{[2]*} - \chi_{[1]}^{[2]}} + \frac{\chi_{[1]}^{[1]*} + \beta_j}{\chi_{[1]}^{[2]} + \beta_j}\frac{1}{\chi_{[1]}^{[1]*} - \chi_{[1]}^{[2]}},\\
a_3^{(j)} &= \frac{\chi_{[1]}^{[1]*} + \beta_j}{\chi_{[1]}^{[1]} + \beta_j}\frac{1}{\chi_{[1]}^{[1]*} - \chi_{[1]}^{[1]}} + \frac{\chi_{[1]}^{[2]*} + \beta_j}{\chi_{[1]}^{[1]} + \beta_j}\frac{1}{\chi_{[1]}^{[2]*} - \chi_{[1]}^{[1]}},\\
a_4^{(j)} &= \frac{\chi_{[1]}^{[2]*} + \beta_j}{\chi_{[1]}^{[1]} + \beta_j}\frac{1}{\chi_{[1]}^{[2]*} - \chi_{[1]}^{[1]}} + \frac{\chi_{[1]}^{[2]*} + \beta_j}{\chi_{[1]}^{[2]} + \beta_j}\frac{1}{\chi_{[1]}^{[2]*} - \chi_{[1]}^{[2]}},
\end{aligned}
\tag{B13}
$$

$$
\begin{aligned}
b_1^{(j)} &= \frac{\chi_{[2]}^{[1]*} + \beta_j}{\chi_{[1]}^{[1]} + \beta_j}\frac{1}{\chi_{[2]}^{[1]*} - \chi_{[1]}^{[1]}} + \frac{\chi_{[2]}^{[2]*} + \beta_j}{\chi_{[1]}^{[1]} + \beta_j}\frac{1}{\chi_{[2]}^{[2]*} - \chi_{[1]}^{[1]}},\\
b_2^{(j)} &= \frac{\chi_{[2]}^{[2]*} + \beta_j}{\chi_{[1]}^{[2]} + \beta_j}\frac{1}{\chi_{[2]}^{[2]*} - \chi_{[1]}^{[2]}} + \frac{\chi_{[2]}^{[1]*} + \beta_j}{\chi_{[1]}^{[2]} + \beta_j}\frac{1}{\chi_{[2]}^{[1]*} - \chi_{[1]}^{[2]}},\\
b_3^{(j)} &= \frac{\chi_{[2]}^{[1]*} + \beta_j}{\chi_{[1]}^{[1]} + \beta_j}\frac{1}{\chi_{[2]}^{[1]*} - \chi_{[1]}^{[1]}} + \frac{\chi_{[2]}^{[2]*} + \beta_j}{\chi_{[1]}^{[1]} + \beta_j}\frac{1}{\chi_{[2]}^{[2]*} - \chi_{[1]}^{[1]}},\\
b_4^{(j)} &= \frac{\chi_{[2]}^{[2]*} + \beta_j}{\chi_{[1]}^{[1]} + \beta_j}\frac{1}{\chi_{[2]}^{[2]*} - \chi_{[1]}^{[1]}} + \frac{\chi_{[2]}^{[2]*} + \beta_j}{\chi_{[1]}^{[2]} + \beta_j}\frac{1}{\chi_{[2]}^{[2]*} - \chi_{[1]}^{[2]}},
\end{aligned}
\tag{B14}
$$

$$
\begin{aligned}
c_1^{(j)} &= \frac{\chi_{[2]}^{[1]*}+\beta_j}{\chi_{[2]}^{[1]}+\beta_j}\frac{1}{\chi_{[2]}^{[1]*}-\chi_{[2]}^{[1]}}+\frac{\chi_{[2]}^{[2]*}+\beta_j}{\chi_{[2]}^{[1]}+\beta_j}\frac{1}{\chi_{[2]}^{[2]*}-\chi_{[2]}^{[1]}},\\
c_2^{(j)} &= \frac{\chi_{[2]}^{[2]*}+\beta_j}{\chi_{[1]}^{[1]}+\beta_j}\frac{1}{\chi_{[2]}^{[2]*}-\chi_{[2]}^{[2]}}+\frac{\chi_{[2]}^{[1]*}+\beta_j}{\chi_{[2]}^{[2]}+\beta_j}\frac{1}{\chi_{[2]}^{[1]*}-\chi_{[2]}^{[2]}},\\
c_3^{(j)} &= \frac{\chi_{[2]}^{[1]*}+\beta_j}{\chi_{[1]}^{[1]}+\beta_j}\frac{1}{\chi_{[2]}^{[1]*}-\chi_{[1]}^{[1]}}+\frac{\chi_{[2]}^{[2]*}+\beta_j}{\chi_{[2]}^{[1]}+\beta_j}\frac{1}{\chi_{[2]}^{[2]*}-\chi_{[2]}^{[1]}},\\
c_4^{(j)} &= \frac{\chi_{[2]}^{[2]*}+\beta_j}{\chi_{[1]}^{[1]}+\beta_j}\frac{1}{\chi_{[2]}^{[2]*}-\chi_{[2]}^{[1]}}+\frac{\chi_{[2]}^{[2]*}+\beta_j}{\chi_{[2]}^{[2]}+\beta_j}\frac{1}{\chi_{[2]}^{[2]*}-\chi_{[2]}^{[2]}},
\end{aligned}
\tag{B15}
$$

Based on the derivation of two-fold DT, the higher-order solutions for the SRBs of Eqs. (1) can be given as

$$
\begin{aligned}
\psi_{\mathrm{SRB}[N]}^{(1)} &= \psi_{2N}^{(1)} = \psi_{2N-1}^{(1)} + (\lambda_{[2N]}^{*} - \lambda_{[2N]})\\
&\quad\times \frac{R_{[2N]}^{[2N-1]*} S_{[2N]}^{[2N-1]}}{\left|R_{[2N]}^{[2N-1]}\right|^2 + \left|S_{[2N]}^{[2N-1]}\right|^2 + \left|W_{[2N]}^{[2N-1]}\right|^2},\\
\psi_{\mathrm{SRB}[N]}^{(2)} &= \psi_{2N}^{(2)} = \psi_{2N-1}^{(2N)} + (\lambda_{[2N]}^{*} - \lambda_{[2N]})\\
&\quad\times \frac{R_{[2N]}^{[2N-1]*} W_{[2N]}^{[2N-1]}}{\left|R_{[2N]}^{[2N-1]}\right|^2 + \left|S_{[2N]}^{[2N-1]}\right|^2 + \left|W_{[2N]}^{[2N-1]}\right|^2},
\end{aligned}
\tag{B16}
$$

where

$$
\begin{aligned}
R_{[2N]}^{[2N-1]} &= T[2N-1]\cdots T[1]T[0]R_{[2N]}^{[0]},\\
S_{[2N]}^{[2N-1]} &= T[2N-1]\cdots T[1]T[0]S_{[2N]}^{[0]},\\
W_{[2N]}^{[2N-1]} &= T[2N-1]\cdots T[1]T[0]W_{[2N]}^{[0]},
\end{aligned}
\tag{B17}
$$

with

$$
\begin{aligned}
T[0] &= I,\\
T[2N-1] &= I + \frac{\lambda_{[2N-1]}^{*} - \lambda_{[2N-1]}}{\lambda_{[2N]} - \lambda_{[2N-1]}^{*}} \frac{\mathbf{\Psi}_{[2N]}^{[2N-1]} \mathbf{\Psi}_{[2N]}^{[2N-1]\dagger}}{\mathbf{\Psi}_{[2N]}^{[2N-1]\dagger} \mathbf{\Psi}_{[2N]}^{[2N-1]}}.
\end{aligned}
\tag{B18}
$$

Such solutions can be also written as the general determinant form of the $2N$th order breather solutions,

$$
\psi_{\mathrm{SRB}[N]}^{(j)} = \psi_{2N}^{(j)} = \psi_0^{(j)} \frac{\det A_j}{\det B},
\tag{B19}
$$

where

$$
A_j = \left(a_{[n_1][n_2]}^{(j)}\right), \quad 1 \leqslant [n_1], [n_2] \leqslant 2N,
\tag{B20}
$$

$$
B = (b_{[n_1][n_2]}), \quad 1 \leqslant [n_1], [n_2] \leqslant 2N,
\tag{B21}
$$

with

$$
\begin{aligned}
a_{[n_1][n_2]}^{(j)} &= \frac{\chi_{[n_2]}^{[1]*}+\beta_j}{\chi_{[n_1]}^{[1]}+\beta_j}\frac{\varphi_{[n_1]}^{[1]}+\varphi_{[n_2]}^{[1]*}}{\chi_{[n_2]}^{[1]*}-\chi_{[n_1]}^{[1]}} + \frac{\chi_{[n_2]}^{[2]*}+\beta_j}{\chi_{[n_1]}^{[1]}+\beta_j}\frac{\varphi_{[n_1]}^{[1]}+\varphi_{[n_2]}^{[2]*}}{\chi_{[n_2]}^{[2]*}-\chi_{[n_1]}^{[1]}}\\
&\quad + \frac{\chi_{[n_2]}^{[1]*}+\beta_j}{\chi_{[n_1]}^{[2]}+\beta_j}\frac{\varphi_{[n_1]}^{[2]*}+\varphi_{[n_2]}^{[1]}}{\chi_{[n_2]}^{[2]*}-\chi_{[n_1]}^{[1]}}\\
&\quad + \frac{\chi_{[n_2]}^{[2]*}+\beta_j}{\chi_{[n_1]}^{[2]}+\beta_j}\frac{\varphi_{[n_1]}^{[2]}+\varphi_{[n_2]}^{[2]*}}{\chi_{[n_2]}^{[2]*}-\chi_{[n_1]}^{[2]}}.
\end{aligned}
\tag{B22}
$$

$$
\begin{aligned}
b_{[n_1][n_2]} &= \frac{\varphi_{[n_1]}^{[1]}+\varphi_{[n_2]}^{[1]*}}{\chi_{[n_2]}^{[1]*}-\chi_{[n_1]}^{[1]}} + \frac{\varphi_{[n_1]}^{[1]}+\varphi_{[n_2]}^{[2]*}}{\chi_{[n_2]}^{[2]*}-\chi_{[n_1]}^{[1]}}\\
&\quad + \frac{\varphi_{[n_1]}^{[2]*}+\varphi_{[n_2]}^{[1]}}{\chi_{[n_2]}^{[2]*}-\chi_{[n_1]}^{[1]}} + \frac{\varphi_{[n_1]}^{[2]}+\varphi_{[n_2]}^{[2]*}}{\chi_{[n_2]}^{[2]*}-\chi_{[n_1]}^{[2]}},
\end{aligned}
\tag{B23}
$$

Here $a_{[n_1][n_2]}^{(j)}$ and $a_{[n_1][n_2]}$ represent the matrix elements of A_j and B in the n_1th row and n_2th column. Moreover, $\chi_{[n_1]}^{[2]}(\chi_{[n_2]}^{[2]}) = \chi_{[n_1]}^{[1]}(\chi_{[n_2]}^{[1]}) + \omega + i\alpha \quad (n_1, n_2 = 1, 2, \ldots, N)$, with $\chi_{[n_1]}^{[1]}(\chi_{[n_2]}^{[1]})$ being one of the complex roots of Eq. (11).

APPENDIX C: PARTICULAR CASE: THE SCALAR SRBs

We consider the scalar Hirota equation in the following form [58]:

$$
i\psi_t + \tfrac{1}{2}\psi_{xx} + |\psi|^2\psi + i\epsilon(\psi_{xxx} + 6|\psi|^2\psi_x) = 0.
\tag{C1}
$$

This equation admits a Lax pair in the linear form

$$
\mathbf{\Psi}_x = \boldsymbol{U}\mathbf{\Psi}, \quad \mathbf{\Psi}_t = \boldsymbol{V}\mathbf{\Psi},
\tag{C2}
$$

where $\mathbf{\Psi} = (R, S)^T$ and

$$
\begin{aligned}
\boldsymbol{U} &= i\begin{pmatrix} \lambda & \psi^* \\ \psi & 0 \end{pmatrix},\\
\boldsymbol{V} &= \lambda^3 V_3 + \lambda^2 V_2 + \lambda V_1 + V_0,
\end{aligned}
\tag{C3}
$$

with

$$
\begin{aligned}
V_3 &= \frac{i}{2}(I+\Lambda), V_2 = \frac{i}{4}(I+\Lambda) + i\epsilon Q,\\
V_1 &= \frac{i}{2}Q + \epsilon\Lambda(Q_x - iQ^2) + i\epsilon\Lambda_0 a^2,\\
V_0 &= \frac{1}{2}\Lambda(Q_x - iQ^2) + \frac{\epsilon}{4}(I-\Lambda)(Q^2 - 2a^2)_x - 3i\epsilon Q a^2,
\end{aligned}
\tag{C4}
$$

and

$$
\Lambda = \begin{pmatrix} 1 & 0 \\ 0 & -1 \end{pmatrix}, \quad \Lambda_0 = \begin{pmatrix} 1 & 0 \\ 0 & -2 \end{pmatrix}, \quad Q = \begin{pmatrix} 0 & \psi^* \\ \psi & 0 \end{pmatrix}.
\tag{C5}
$$

For a general breather in Eq. (C1), the eigenvalue $\boldsymbol{\chi}$ associated with the Lax pair (C2) satisfies the relation

$$
1 + \frac{a^2}{(\boldsymbol{\chi}+\beta)(\boldsymbol{\chi}+\omega+i\alpha)} = 0,
\tag{C6}
$$

with a and β being the amplitude and wave number of the scalar background plane wave

$$
\psi_0 = a\exp\left\{i\beta x + i\left[a^2 - \frac{\beta^2}{2} + \epsilon(\beta^3 - 6a^2\beta)\right]t\right\},
$$

and ϵ is the higher-order coefficient. Parameters ω and α are two real constants which have been defined in the vector case above. The spectral parameter λ obeys the following relation with the eigenvalue $\boldsymbol{\chi}$:

$$
\lambda = \boldsymbol{\chi} - \frac{a^2}{\boldsymbol{\chi}+\beta}.
\tag{C7}
$$

From Eq. (C6), one can obtain

$$\chi_1 = -\frac{\omega}{2} - \frac{i\alpha}{2} - \beta + \sqrt{\frac{\omega^2-\alpha^2}{4} + \frac{i\alpha\omega}{2} - a^2},$$
$$\chi_2 = -\frac{\omega}{2} - \frac{i\alpha}{2} - \beta - \sqrt{\frac{\omega^2-\alpha^2}{4} + \frac{i\alpha\omega}{2} - a^2}. \quad \text{(C8)}$$

As a result, according to Eq. (C7), the spectral parameter λ can be given as

$$\lambda_1 = -\frac{\omega+i\alpha}{2} - \beta + \sqrt{\frac{\omega^2-\alpha^2}{4} + \frac{i\alpha\omega}{2} - a^2} + \frac{a^2}{\frac{\omega+i\alpha}{2} - \sqrt{\frac{\omega^2-\alpha^2}{4} + \frac{i\alpha\omega}{2} - a^2}},$$
$$\lambda_2 = -\frac{\omega+i\alpha}{2} - \beta - \sqrt{\frac{\omega^2-\alpha^2}{4} + \frac{i\alpha\omega}{2} - a^2} - \frac{a^2}{\frac{\omega+i\alpha}{2} + \sqrt{\frac{\omega^2-\alpha^2}{4} + \frac{i\alpha\omega}{2} - a^2}}. \quad \text{(C9)}$$

Such two spectral parameters adhere to the following relations:

$$\lambda_{1r} + \lambda_{2r} = -2\beta, \quad \lambda_{1i} + \lambda_{2i} = 0, \quad \text{(C10)}$$

which bear similarities to the case of the scalar NLSE, and the first relation has also been given in Ref. [46].

Using onefold DT, one can easily obtain the fundamental solutions $\psi_1(x,t)$ for Eq. (C1),

$$\psi_1 = \psi_0 + \left(\lambda^*_{[1]} - \lambda_{[1]}\right)\frac{R[1]^* S[1]}{|R[1]|^2 + |S[1]|^2}, \quad \text{(C11)}$$

where

$$R[1] = \varphi^{[1]}_{[1]} + \varphi^{[2]}_{[1]}, \quad S[1] = \psi_0\left(\frac{\varphi^{[1]}_{[1]}}{\chi+\beta} + \frac{\varphi^{[2]}_{[1]}}{\chi-\beta}\right), \quad \text{(C12)}$$

with

$$\varphi^{[1]}_{[1]} = a\exp\left\{i\chi^{[1]}_{[1]}x + i\left[\epsilon\chi^{[1]3}_{[1]} + \frac{\chi^{[1]2}_{[1]}}{2} - 2\epsilon a^2\chi^{[1]}_{[1]} - \epsilon a^2\right]t\right\},$$
$$\varphi^{[2]}_{[1]} = a\exp\left\{i\chi^{[2]}_{[1]}x + i\left[\epsilon\chi^{[2]3}_{[1]} + \frac{\chi^{[2]2}_{[1]}}{2} - 2\epsilon a^2\chi^{[2]}_{[1]} - \epsilon a^2\right]t\right\}. \quad \text{(C13)}$$

Here, $\chi^{[1]}_{[1]}$ is one of the eigenvalues in Eq. (C8) and $\chi^{[2]}_{[1]} = \chi^{[1]}_{[1]} + \omega + i\alpha$. When α is nonzero but small, namely, $0 < \alpha \ll 1$, the solution is the quasi-AB corresponding the spectral parameter $\lambda_{[1]} = \chi^{[1]}_{[1]} - \frac{a^2}{\chi^{[1]}_{[1]}+\beta}$. The nonlinear superposition of two quasi-ABs corresponding to two different spectral parameters can be used to generate the fundamental scalar SRB,

$$\psi_{\mathrm{SRB}[1]} = \psi_2 = \psi_1 + (\lambda^*_{[2]} - \lambda_{[2]})\frac{R^{[1]*}_{[2]} S^{[1]}_{[2]}}{\left|R^{[1]}_{[2]}\right|^2 + \left|S^{[1]}_{[2]}\right|^2}, \quad \text{(C14)}$$

where

$$R^{[1]}_{[2]} = T[1]R^{[0]}_{[2]}, \quad S^{[1]}_{[2]} = T[1]S^{[0]}_{[2]}, \quad \text{(C15)}$$

with

$$T[1] = I + \frac{\lambda^*_{[1]} - \lambda_{[1]}}{\lambda_{[2]} - \lambda^*_{[1]}}\frac{\mathbf{\Psi}[1]^\dagger\mathbf{\Psi}[1]}{\mathbf{\Psi}[1]\mathbf{\Psi}[1]^\dagger},$$
$$R^{[0]}_{[2]} = \varphi^{[1]}_{[2]} + \varphi^{[2]}_{[2]},$$
$$S^{[0]}_{[2]} = \psi_0\left(\frac{\varphi^{[1]}_{[2]}}{\chi+\beta} + \frac{\varphi^{[2]}_{[2]}}{\chi-\beta}\right). \quad \text{(C16)}$$

The above results can also be obtained based on the Jukowsky transform for the spectral parameter λ, which have been provided in Ref. [46]. Here, we recall the calculation process. For simplicity, we take a rogue wave as the starting point. In fact, when $\alpha = \omega = 0$, the corresponding spectral parameter is a special one that obeys the relation

$$1 + \frac{a^2}{(\chi+\beta)^2} = 0. \quad \text{(C17)}$$

Each of such eigenvalues corresponds to the scalar rogue wave solution in Eq. (C1) and their explicit expressions The explicit expressions for them are detailed as follows:

$$\chi_1 = -\beta + ia, \quad \chi_2 = -\beta - ia. \quad \text{(C18)}$$

The corresponding spectral parameters are expressed as

$$\lambda_1 = -\beta + 2ia, \quad \lambda_2 = -\beta - 2ia. \quad \text{(C19)}$$

Since the signs of the imaginary parts of λ_1, λ_2 have no effects on the nonlinear wave, without loss of generality, we choose λ_1 for the following analysis. After performing the Jukowsky transformation, one of the spectral parameters that can be used to generate the SRB is expressed as

$$\lambda(R,\theta) = \frac{i}{2}\left(\xi + \frac{1}{\xi}\right)\mathrm{Im}(\lambda) + \mathrm{Re}(\lambda), \quad \text{(C20)}$$

with

$$\xi = R\exp(i\theta). \quad \text{(C21)}$$

Parameters R and θ represent the radius and angle of the polar coordinates in the sector $\mathcal{D} = \{R = 1, \theta \in (-\pi/2, \pi/2)\}$. Then one has

$$\lambda(R,\theta) = ia\left(R + \frac{1}{R}\right)\cos\theta - \beta - a\left(R - \frac{1}{R}\right)\sin\theta. \quad \text{(C22)}$$

Therefore, one can easily obtain the expression of λ for the general breathers in the similar form

$$\lambda(r,\theta) = ia\left(r + \frac{1}{r}\right)\cos\theta - \beta - a\left(r - \frac{1}{r}\right)\sin\theta, \quad \text{(C23)}$$

where $r = (1+\varepsilon)R \geqslant 1$. Consequently, one obtains

$$\lambda_{1r} = \mathrm{Re}[\lambda(r,\theta)] = -\beta - a\left(r - \frac{1}{r}\right)\sin\theta,$$
$$\lambda_{1i} = \mathrm{Im}[\lambda(r,\theta)] = ia\left(r\frac{1}{r}\right)\cos\theta,$$
$$\lambda_{2r} = \mathrm{Re}[\lambda(-r,\theta)] = -\beta + a\left(r - \frac{1}{r}\right)\sin\theta,$$
$$\lambda_{2i} = \mathrm{Im}[\lambda(r,\theta)] = ia\left(r + \frac{1}{r}\right)\cos\theta.$$

[1] N. Akhmediev and A. Ankiewicz, *Nonlinear Pulses and Beams* (Springer, Berlin, 1997).

[2] J. M. Dudley, F. Dias, M. Erkintalo, and G. Genty, Instabilities, breathers and rogue waves in optics, Nat. Photonics **8**, 755 (2014).

[3] J. M. Dudley, G. Genty, F. Dias, B. Kibler, and N. Akhmediev, Modulation instability, Akhmediev breathers and continuous wave supercontinuum generation, Opt. Express **17**, 21497 (2009).

[4] A. Chabchoub, N. P. Hoffmann, and N. Akhmediev, Rogue wave observation in a water wave tank, Phys. Rev. Lett. **106**, 204502 (2011).

[5] B. Frisquet, B. Kibler, and G. Millot, Collision of Akhmediev breathers in nonlinear fiber optics, Phys. Rev. X **3**, 041032 (2013).

[6] G. Xu, A. Gelash, A. Chabchoub, V. Zakharov, and B. Kibler, Breather wave molecules, Phys. Rev. Lett. **122**, 084101 (2019).

[7] A. Chabchoub, N. Hoffmann, M. Onorato, and N. Akhmediev, Super rogue waves: Observation of a higher-order breather in water waves, Phys. Rev. X **2**, 011015 (2012).

[8] V. E. Zakharov and A. A. Gelash, Nonlinear stage of modulation instability, Phys. Rev. Lett. **111**, 054101 (2013).

[9] A. Chabchoub, M. Onorato, and N. Akhmediev, Hydrodynamic envelope solitons and breathers, in *Rogue and Shock Waves in Nonlinear Dispersive Media* (Springer, Berlin, 2016), pp. 55–87.

[10] M. Närhi, B. Wetzel, C. Billet, S. Toenger, T. Sylvestre, J. M. Merolla, R. Morandotti, F. Dias, G. Genty, and J. M. Dudley, Real-time measurements of spontaneous breathers and rogue wave events in optical fibre modulation instability, Nat. Commun. **7**, 13675 (2016).

[11] N. Akhmediev, A. Ankiewicz, and J. M. Soto-Crespo, Fundamental rogue waves and their superpositions in nonlinear integrable systems, in *Nonlinear Guided Wave Optics: A Testbed for Extreme Waves* (IOP, Bristol, 2017), pp. 10-1.

[12] A. Tikan, S. Bielawski, C. Szwaj, S. Randoux, and P. Suret, Single-shot measurement of phase and amplitude by using a heterodyne time-lens system and ultrafast digital time-holography, Nat. Photonics **12**, 228 (2018).

[13] C. Liu, Z. Y. Yang, W. L. Yang, and N. Akhmediev, Chessboard-like spatio-temporal interference patterns and their excitation, J. Opt. Soc. Am. B **36**, 1294 (2019).

[14] N. Akhmediev and V. I. Korneev, Modulation instability and periodic solutions of the nonlinear Schrödinger equation, Theor. Math. Phys. **69**, 1089 (1986).

[15] N. Akhmediev, V. M. Eleonskii, and N. E. Kulagin, Exact first-order solutions of the nonlinear Schrödinger equation, Theor. Math. Phys. **72**, 809 (1987).

[16] V. E. Zakharov and L. A. Ostrovsky, Modulation instability: The beginning, Physica D **238**, 540 (2009).

[17] E. A. Kuznetsov, Solitons in a parametrically unstable plasma, Sov. Phys. Dokl. **22**, 507 (1977).

[18] Y. C. Ma, The perturbed plane-wave solutions of the cubic Schrödinger equation, Stud. Appl. Math. **60**, 43 (1979).

[19] M. Conforti, A. Mussot, A. Kudlinski, S. Trillo, and N. Akhmediev, Doubly periodic solutions of the focusing nonlinear Schrödinger equation: Recurrence, period doubling, and amplification outside the conventional modulation instability band, Phys. Rev. A **101**, 023843 (2020).

[20] D. H. Peregrine, Water waves, nonlinear Schrödinger equations and their solutions, J. Aust. Math. Soc. Ser. B **25**, 16 (1983).

[21] N. Akhmediev, A. Ankiewicz, and M. Taki, Waves that appear from nowhere and disappear without a trace, Phys. Lett. A **373**, 675 (2009).

[22] A. Gelash and A. Raskovalov, Vector breathers in the Manakov system, Stud. Appl. Math. **150**, 841 (2023).

[23] D. Agafontsev, A. Gelash, S. Randoux, and P. Suret, Multisoliton interactions approximating the dynamics of breather solutions, Stud. Appl. Math. **152**, 810 (2024).

[24] A. A. Gelash and V. E. Zakharov, Superregular solitonic solutions: A novel scenario for the nonlinear stage of modulation instability, Nonlinearity **27**, R1 (2014).

[25] B. Kibler, A. Chabchoub, A. Gelash, N. Akhmediev, and V. E. Zakharov, Superregular breathers in optics and hydrodynamics: Omnipresent modulation instability beyond simple periodicity, Phys. Rev. X **5**, 041026 (2015).

[26] V. I. Bespalov and V. I. Talanov, Filamentary structure of light beams in nonlinear liquids, JETP Lett. **3**, 307 (1966).

[27] L. Duan, L. C. Zhao, W. H. Xu, C. Liu, Z. Y. Yang, and W. L. Yang, Soliton excitations on a continuous-wave background in the modulational instability regime with fourth-order effects, Phys. Rev. E **95**, 042212 (2017).

[28] L. C. Zhao and L. M. Ling, Quantitative relations between modulational instability and several well-known nonlinear excitations, J. Opt. Soc. Am. B **33**, 850 (2016).

[29] L. M. Ling, L. C. Zhao, Z. Y. Yang, and B. L. Guo, Generation mechanisms of fundamental rogue wave spatial-temporal structure, Phys. Rev. E **96**, 022211 (2017).

[30] F. Baronio, S. H. Chen, P. Grelu, S. Wabnitz, and M. Conforti, Baseband modulation instability as the origin of rogue waves, Phys. Rev. A **91**, 033804 (2015).

[31] F. Baronio, M. Conforti, A. Degasperis, S. Lombardo, M. Onorato, and S. Wabnitz, Vector rogue waves and baseband modulation instability in the defocusing regime, Phys. Rev. Lett. **113**, 034101 (2014).

[32] S. H. Chen, F. Baronio, J. Soto-Crespo, P. Grelu, M. Conforti, and S. Wabnitz, Optical rogue waves in parametric three-wave mixing and coherent stimulated scattering, Phys. Rev. A **92**, 033847 (2015).

[33] M. Erkintalo, K. Hammani, B. Kibler, C. Finot, N. Akhmediev, J. M. Dudley, and G. Genty, Higher-order modulation instability in nonlinear fiber optics, Phys. Rev. Lett. **107**, 253901 (2011).

[34] C. Liu, Y. Ren, Z. Y. Yang, and W. L. Yang, Superregular breathers in a complex modified Korteweg–de Vries system, Chaos **27**, 083120 (2017).

[35] G. Biondini and E. Fagerstrom, The integrable nature of modulational instability, SIAM J. Appl. Math. **75**, 136 (2015).

[36] G. Biondini, S. Li, and D. Mantzavinos, Oscillation structure of localized perturbations in modulationally unstable media, Phys. Rev. E **94**, 060201(R) (2016).

[37] G. Biondini and D. Mantzavinos, Universal nature of the nonlinear stage of modulational instability, Phys. Rev. Lett. **116**, 043902 (2016).

[38] G. Biondini and D. Mantzavinos, Long-time asymptotics for the focusing nonlinear Schrödinger equation with nonzero boundary conditions at infinity and asymptotic stage of modulational instability, Commun. Pure Appl. Math. **70**, 2300 (2017).

[39] C. Liu, L. Wang, Z. Y. Yang, and W. L. Yang, Femtosecond optical superregular breathers, arXiv:1708.03781.

[40] J. H. Zhang, L. Wang, and C. Liu, Superregular breathers, characteristics of nonlinear stage of modulation instability induced by higher-order effects, Proc. R. Soc. A **473**, 20160681 (2017).

[41] C. Liu, Z. Y. Yang, and W. L. Yang, Growth rate of modulation instability driven by superregular breathers, Chaos: An Interdiscip. J. Nonlinear Sci. **28**, 083110 (2018).

[42] Y. Ren, X. Wang, C. Liu, Z. Y. Yang, and W. L. Yang, Characteristics of fundamental and superregular modes in a multiple self-induced transparency system, Commun. Nonlinear Sci. Numer. Simulat. **63**, 161 (2018).

[43] C. Liu and N. Akhmediev, Super-regular breathers in nonlinear systems with self-steepening effect, Phys. Rev. E **100**, 062201 (2019).

[44] Y. Ren, Z. Y. Yang, C. Liu, and W. L. Yang, Controllable optical superregular breathers in the femtosecond regime, Chin. Phys. B **27**, 010504 (2018).

[45] Y. Ren, C. Liu, Z. Y. Yang, and W. L. Yang, Polariton superregular breathers in a resonant erbium-doped fiber, Phys. Rev. E **98**, 062223 (2018).

[46] C. Liu, S. C. Chen, and N. Akhmediev, Fundamental and second-order superregular breathers in vector fields, Phys. Rev. Lett. **132**, 027201 (2024).

[47] L. H. Wang, K. Porsezian, and J. S. He, Breather and rogue wave solutions of a generalized nonlinear Schrödinger equation, Phys. Rev. E **87**, 053202 (2013).

[48] X. Wang, B. Yang, Y. Chen, and Y. Q. Yang, Higher-order rogue wave solutions of the Kundu-Eckhaus equation, Phys. Scr. **89**, 095210 (2014).

[49] R. S. Tasgal and M. J. Potasek, Soliton solutions to coupled higher-order nonlinear Schrödinger equations, J. Math. Phys. **33**, 1208 (1992).

[50] A. Ankiewicz, J. M. Soto-Crespo, and N. Akhmediev, Rogue waves and rational solutions of the hirota equation, Phys. Rev. E **81**, 046602 (2010).

[51] S. H. Chen and D. Mihalache, Vector rogue waves in the Manakov system: Diversity and compossibility, J. Phys. A: Math. Theor. **48**, 215202 (2015).

[52] G. P. Agrawal, Nonlinear fiber optics, in *Nonlinear Science at the Dawn of the 21st Century* (Springer, Berlin, 2000), pp. 195–211.

[53] P. G. Kevrekidis, D. J. Frantzeskakis, and R. Carretero-González, *Emergent Nonlinear Phenomena in Bose-Einstein Condensates: Theory and Experiment* (Springer, Berlin, 2008).

[54] S. H. Chen, Dark and composite rogue waves in the coupled Hirota equations, Phys. Lett. A **378**, 2851 (2014).

[55] C. Liu, Z. Y. Yang, L. C. Zhao, and W. L. Yang, State transition induced by higher-order effects and background frequency, Phys. Rev. E **91**, 022904 (2015).

[56] V. B. Matveev and M. A. Salle, *Darboux Transformations and Solitons*, Springer Series in Nonlinear Dynamics (Springer, Berlin, 1991).

[57] C. Liu, Z. Y. Yang, L. C. Zhao, and W. L. Yang, Transition, coexistence, and interaction of vector localized waves arising from higher-order effects, Ann. Phys. (NY) **362**, 130 (2015).

[58] R. Hirota, Exact envelope-soliton solutions of a nonlinear wave equation, J. Math. Phys. **14**, 805 (1973).